Universidad del País Vasco
Euskal Herriko Unibertsitatea

ZIENTZIA ETA TEKNOLOGIA FAKULTATEA
FACULTAD DE CIENCIA Y TECNOLOGÍA

Gradu amaierako lana / Trabajo fin de grado
Fisikako gradua/ Grado en Física

Analysis of Plasmonic Nanostructures Using the Quasinormal Mode Formalism

Egilea / Autor/a:
Xabier Arrieta Aristi

Zuzendaria / Director/a:
Ruben Esteban Llorente (CSIC)
Miren Nerea Zabala Unzalu (EHU/UPV)

© 2021, Xabier Arrieta Aristi

Leioa, 2021eko ekainaren 18a / Leioa, 18 de junio de 2021

Contents

1 Overview and objectives of the work

In the last decades, nanophotonics (control of light at the nanoscale) has witnessed a great revolution, which has largely been due to innovative fabrication techniques, increasing computational capabilities and improving theoretical understanding. A field of great interest in nanophotonics is the area of plasmonics, which studies how the incident electromagnetic fields excite the collective oscillation of conduction electrons on noble metals (especially silver and gold). This collective oscillation can be understood as a quasiparticle called plasmon [1]. It is believed that the first application of plasmonics dates to the Roman era, the Lycurgus cup. This cup contains nanoparticles made of a silver-gold alloy, which explain its colours. Nonetheless, it was not until the second half of the 20th century that plasmonics became a viable source of study with the discovery of surface plasmon polaritons [2]. Since then, the field is in a constant change finding new innovative applications [3].

The collective oscillation of the electrons is able to enhance the field near the surface of the metal. This field enhancement can for example be used to study single molecules, which is often not possible in a standard setup because the emitted light is too weak. Further, plasmons are able to confine light beyond the diffraction limit, that is, they enable to get a better field localisation than half of the wavelength. These characteristics of plasmons have led to different applications, not only in physics but also in chemistry and biology. For instance, an application that has attracted much attention is surface-enhanced Raman scattering, which takes advantage of the field enhancement produced by plasmons to study molecular vibrations [4]. Furthermore, field enhancement can also be used to intensify molecular fluorescence, which facilitates the detection of single molecules. Beyond the ability to confine light, metallic nanostructures can absorb light and convert it to heat due to losses, heating the metallic nanoparticle and the surrounding media. This heating could be used to enhance chemical reactions and for drug delivery [5]. Also, it can be used to achieve selective heating in planar structures to change the magnetic properties of nanomagnets, which is much faster and energetically more efficient than the classical methods where a hot reservoir is commonly used [6].

The response of plasmonic structures depends strongly on the geometry of the system, so that in order to optimise the applications, it is essential to calculate how a system will respond to an applied electromagnetic excitation. This is usually achieved by resolving Maxwell's equations since for most systems classical calculations are sufficient and there is no need to consider quantum corrections. Generally, it is very challenging to calculate the exact analytical solution of Maxwell's equations, except for simple systems such as a sphere. Thus, numerous computational methods have been developed to get the response of arbitrary structures, including the finite element method (FEM), finite difference time domain method (FDTD) and boundary element method (BEM) among some others. In this work, it was decided to focus on the finite element method to solve the optical response of the plasmonic nanostructures of interest.

FEM simulations usually give the response of a system when it is illuminated with a specific laser. Although the results are very precise, sometimes the understanding of the spectra can be complicated. The response of plasmonic structures is usually composed by different resonances and it is very interesting to differentiate their contribution because it

allows a better physical understanding. Nonetheless, if two resonances are spectrally very close it can be a challenging task to separate the contribution of each one using only the FEM spectra. Furthermore, in FEM simulations Maxwell's equations need to be solved for each incident field. In some cases, a study of different excitations is needed, for example changing the direction of an incident wave or changing the position of dipolar excitation sources, which can be very time demanding simulations. In this context, a new formalism was developed recently, called quasinormal mode (QNM) formalism. The main principle is to resolve the Maxwell's equations without any incident field, which are called source-free Maxwell's equations. Thus, the problem consists in an eigenvalue and eigenfunction problem. The eigenvectors of the system are called quasinormal modes and have complex eigenvalues which are the frequencies of the QNMs. To each quasinormal mode correspond a resonance, which is excited or not depending on the incident electromagnetic wave.

Different approaches have been developed to work with quasinormal modes [7]. We specifically use an implementation that defines auxiliary fields and perfectly matched layers (PMLs) in order to resolve the eigenvalue problem [8]. The goal of the project is to get familiar with the method and then use it to analyse plasmonic structures of current interest in nanophotonics, such as a nanoparticle on a mirror (NPoM). A NPoM structure is formed by a metallic nanoparticle deposited in a metallic substrate with a nanometric dielectric gap between them. The nanometric gap enables to enhance the fields more strongly than for typical single particle structures.

We introduce the field of plasmonics in section 2. We first present briefly the Maxwell's equations and introduce the Drude-Lorentz model to describe the permittivity of a metal. Afterwards, we use the quasi-static theoretical approach to obtain simple analytical expressions of the response of a metallic nanosphere. From these results, we describe the main properties of plasmons, such as field enhancement and field localisation. We then introduce in section 3 the finite element method and illustrate its capabilities by calculating computationally the electromagnetic response of a sphere, and by comparing it to the approximated results of section 2. In section 4 we explain the general properties of the electromagnetic response of the NPoM structures. FEM simulations are used to analyse their response. Further, we describe the QNM formalism in section 5 and use it to calculate the results for a simple sphere, which we compare to the FEM results. To improve the computational calculations we also describe an approach that can be used for axially symmetric geometries. Last, in section 6 we present and analyse the QNM results for the NPoM, comparing them to FEM simulations.

2 Introduction to plasmonics

Plasmons are quantum quasi-particles that are due to collective oscillations of the conduction electrons in metallic systems. However, in most cases quantum effects are negligible and it is sufficient to solve Maxwell's equations for homogeneous media. We can distinguish two types of plasmons, bulk plasmons and surface plasmons. It is generally not possible to excite bulk plasmons with light. In this work, we are going to centre on surface plasmons polaritons, which result from the interaction of the electromagnetic field with the conduction electrons on the surface of noble metals. Further, there are two different types of surface plasmons, propagating surface plasmon polaritons and localised surface plasmon polaritons. The first appears at the infinite interface between a metallic surface and a dielectric, and consists in a surface wave propagating like an evanescent wave. The localised surface plasmon polaritons are excited at finite plasmonic nanostructures. They are confined near the particle and do not propagate. In this work we are going to consider 3D plasmonic nanocavities, thus, we are going to focus on localised surface plasmon polaritons.

2.1 Classical treatment

The first step to study the plasmons of a specific system is to solve Maxwell's equations. Maxwell's equations for homogeneous and linear media without free charges and currents can be written as [9]

$$\nabla \cdot \mathbf{D}(\mathbf{r},t) = 0, \tag{1a}$$

$$\nabla \cdot \mathbf{B}(\mathbf{r},t) = 0\ , \tag{1b}$$

$$\nabla \times \mathbf{E}(\mathbf{r},t) = -\frac{\partial \mathbf{B}(\mathbf{r},t)}{\partial t}\ , \tag{1c}$$

$$\nabla \times \mathbf{H}(\mathbf{r},t) = \frac{\partial \mathbf{D}(\mathbf{r},t)}{\partial t}\ . \tag{1d}$$

The H field ($\mathbf{H}$) and the magnetic field ($\mathbf{B}$) are related with each other via the permeability constant (μ). Since we are working with non-magnetic materials the relation between them is simply $\mathbf{B}(\mathbf{r},t) = \mu_0\mathbf{H}(\mathbf{r},t)$, μ_0 being the vacuum permeability. Similarly, the coefficient which relates the electric displacement ($\mathbf{D}$) and the electric field ($\mathbf{E}$) is the permittivity of the material (ϵ). For simple media, which is the case of typical dielectrics, the electric field and displacement can be approximately related as $\mathbf{D}(\mathbf{r},t) = \varepsilon_0\varepsilon_r\mathbf{E}(\mathbf{r},t)$, ε_0 being the vacuum permittivity and ε_r the relative permittivity of the material. However, for metallic structures the relation between $\mathbf{D}$ and $\mathbf{E}$ is not so simple due to time retardation effects (subsection 2.2).

Since our systems are constituted by different materials, the Maxwell's equations need to be complemented by some boundary conditions

$$\begin{aligned} D_1^{\perp}(\mathbf{r},t) - D_2^{\perp}(\mathbf{r},t) &= 0\ , & E_1^{\parallel}(\mathbf{r},t) - E_2^{\parallel}(\mathbf{r},t) &= 0\ , \\ B_1^{\perp}(\mathbf{r},t) - B_2^{\perp}(\mathbf{r},t) &= 0\ , & H_1^{\parallel}(\mathbf{r},t) - H_2^{\parallel}(\mathbf{r},t) &= 0\ . \end{aligned} \tag{2}$$

Each subscript (1 or 2) represent one of the two domains forming the boundary, whereas the symbols $\perp$ and $\parallel$ mean the perpendicular and parallel components of the field with respect to the boundary.

2.2 Permittivity of metals

For many materials, such as metals, the polarisation at time t depends on the electric field at previous times, that is, we have a retardation in the polarisation of the material (time non-locality). In this case, $\mathbf{D}$ needs to be related to $\mathbf{E}$ as a convolution with the relative permittivity [10],

$$\mathbf{D}(\mathbf{r},t) = \varepsilon_0 \int \varepsilon_r(\mathbf{r}, t-t')\mathbf{E}(\mathbf{r}',t')\mathrm{d}t' \ . \tag{3}$$

Non-locality in space, which would require a similar equation in space, is usually negligible and not considered here.

In order to avoid working with equation 3 we can use the Fourier transforms and inverse Fourier transforms,

$$\mathbf{f}(\mathbf{r},\omega) = \int_{-\infty}^{\infty} \mathbf{f}(\mathbf{r},t)e^{i\omega t}\mathrm{d}t \qquad \mathbf{f}(\mathbf{r},t) = \int_{-\infty}^{\infty} \mathbf{f}(\mathbf{r},\omega)e^{-i\omega t}\mathrm{d}\omega \ . \tag{4}$$

Since a Fourier transform of a convolution becomes a multiplication we have $\mathbf{D}(\mathbf{r},\omega) = \epsilon(\omega)\mathbf{E}(\mathbf{r},\mathbf{t})$. Thus, working in the frequency domain, Maxwell's equations simplify to

$$\nabla \cdot \mathbf{E}(\mathbf{r},\omega) = 0 \ , \tag{5a}$$

$$\nabla \cdot \mathbf{B}(\mathbf{r},\omega) = 0 \ , \tag{5b}$$

$$\nabla \times \mathbf{E}(\mathbf{r},\omega) = i\omega\mathbf{B}(\mathbf{r},\omega) \ , \tag{5c}$$

$$\nabla \times \mathbf{B}(\mathbf{r},\omega) = -\varepsilon_0\varepsilon_r(\omega)\mu_0 i\omega\mathbf{E}(\mathbf{r},\omega) \ , \tag{5d}$$

with boundary condition written as

$$\begin{aligned} &\varepsilon_{r,1}(\omega)E_1^{\perp}(\mathbf{r},\omega) - \varepsilon_{r,2}(\omega)E_2^{\perp}(\mathbf{r},\omega) = 0 \ , && E_1^{\parallel}(\mathbf{r},\omega) - E_2^{\parallel}(\mathbf{r},\omega) = 0 \ , \\ &B_1^{\perp}(\mathbf{r},\omega) - B_2^{\perp}(\mathbf{r},\omega) = 0 \ , && H_1^{\parallel}(\mathbf{r},\omega) - H_2^{\parallel}(\mathbf{r},\omega) = 0 \ . \end{aligned} \tag{6}$$

2.2.1 Drude model

The electrons of a metal can be divided in a simple picture into two families, conduction electrons and bound electrons. In a first approximation it can be supposed that only conduction electrons (assumed free) contribute to the permittivity of the metal. The Drude model proposes an equation of motion for these free electrons inside a metal [11],

$$\frac{\mathrm{d}\mathbf{p}(t)}{\mathrm{d}t} = -\frac{\mathbf{p}(t)}{\tau} + \mathbf{f}_{\mathrm{ext}}(t) \ . \tag{7}$$

In this equation $\mathbf{f}_{\mathrm{ext}}(t) = -e\mathbf{E}$ is the external force, where $\mathbf{E}(t)$ is the incident electric field, τ is the mean relaxation time and $\mathbf{p}(t)$ is the mean lineal momentum of the electrons. Introducing the electron mass (m) and the electron mean position ($\mathbf{r}(t)$) a second grade equation is obtained after noting that $\mathbf{p}(t) = m\mathbf{r}(t)$,

$$m\frac{\mathrm{d}^2\mathbf{r}(t)}{\mathrm{d}t^2} + \frac{m}{\tau}\frac{\mathrm{d}\mathbf{r}(t)}{\mathrm{d}t} = -e\mathbf{E}(t) \ . \tag{8}$$

Taking the Fourier transform of this equation we get

$$-m\omega^2\mathbf{r}_0(\omega) - \frac{m}{\tau}i\omega\mathbf{r}_0(\omega) = -e\mathbf{E_0}(\omega) \ . \tag{9}$$

Each electron, located at mean distance $\mathbf{r}_0(\omega)$ from the equilibrium, produces a mean electric dipole moment $\mathbf{p}_e(\omega) = -e\mathbf{r}_0(\omega)$. Thus, to calculate the macroscopic polarisation density we need to multiply $\mathbf{p}_e(\omega)$ by the electron density n, $\mathbf{P}(\omega) = -ne\mathbf{r}(\omega)$. Using the relationship between the electric field and the polarisation $\mathbf{P}(\omega) = \varepsilon_0(\varepsilon_r(\omega) - 1)\mathbf{E}(\omega)$, the permittivity of Drude for metals can be deduced,

$$\varepsilon_r(\omega) = 1 - \frac{\omega_p^2}{\omega^2 + i\gamma\omega} \,, \tag{10}$$

where $\omega_p^2 = \frac{ne^2}{m\varepsilon_0}$ and $\gamma = \frac{1}{\tau}$. Although the Drude permittivity is very useful we can introduce two main corrections. Equation 10 was obtained assuming that the conduction electrons are free, however, they are distributed in bands. Thus, the first corrections can be introduced considering an effective mass for the electrons. Further, we can consider the effect of the bound electrons on the permittivity, as discussed in the next subsection.

2.2.2 Drude-Lorentz model: description of interband transitions

When the energy of the photons is large enough, the excitation of bound electrons lead to interband transitions. Classically the bound electrons of a band can be represented similarly as free electrons but adding a restoring force [10],

$$m\frac{\mathrm{d}^2\mathbf{r}(t)}{\mathrm{d}t^2} + m\gamma\frac{\mathrm{d}\mathbf{r}(t)}{\mathrm{d}t} + m\omega_0^2\mathbf{r}(t) = -e\mathbf{E}(t) \,. \tag{11}$$

This equation leads to adding a Lorentz oscillator term to the permittivity,

$$\frac{\omega_p^2}{\omega^2 - \omega_0^2 + i\gamma\omega} \,. \tag{12}$$

In order to generalise for all possible transitions more Lorentzian terms and a constant contribution (ε_∞) can be added to the permittivity function. Taking all terms into account the final permittivity function can be written as

$$\varepsilon_r(\omega) = \varepsilon_\infty \left(1 - \frac{\omega_{p,1}^2}{\omega^2 + i\gamma_1\omega} - \sum_{i=2}^{N} \frac{\omega_{p,i}^2}{\omega^2 - \omega_{0,i}^2 + i\gamma_i\omega} \right) \,, \tag{13}$$

which is called Drude-Lorentz permittivity. This equation shows that metallic materials are strongly dispersive media, that is, the permittivity of the metals depends strongly on the frequency.

The effective masses, relaxation constants and damping constants of the electrons in the bands can in principle be calculated. However, they are usually deduced from experimental results. In this work, we mostly use the experimental results obtained by Johnson and Christy [12] for gold and silver. The Drude-Lorentz permittivity is used in the QNM calculations since they enable to work with complex frequencies (subsection 5.1).

2.3 Localised surface plasmon polaritons

As introduced previously, localised surface plasmon polaritons (plasmons for brevity in the following) are resonances that appear in the electromagnetic response of metallic nanostructures. To discuss their properties, we consider in the section a small metallic sphere. In this case, the quasi-static approximation can be implemented to obtain simple equations, which facilitates the understanding of some of the more important properties of plasmons.

2.3.1 Quasi-static approximation of the optical response of a metallic nanosphere

The quasi-static approximation consists in assuming that the field derivatives respect to time are much smaller than the gradient of the fields. In this approximation valid for small particles, the time derivatives of the fields can be set to zero. According to equation 1c the curl of the electric field is then also zero. Since the curl of the electric field is zero, a electric potential can be defined as $\mathbf{E} = -\nabla\phi$ [13]. Introducing this potential in the frequency domain Maxwell's equation 5a, the problem simplifies to a single second grade equation, called Laplace equation,

$$\nabla \cdot \mathbf{E}(\mathbf{r},\omega) = 0 \quad \longrightarrow \quad \nabla^2\phi(\mathbf{r},\omega) = 0\ . \tag{14}$$

In the work we consider illumination by a plane wave, which in the quasi-static approximation is simplified to a constant field, $\mathbf{E}_{\text{inc}}(\mathbf{r}) = E_0 e^{ik_x x}\hat{\mathbf{z}} \approx E_0\hat{\mathbf{z}} = \mathbf{E}_0$. This approximation gives good results when the wavelength λ of the incoming wave is much greater than the dimension of the sphere, that is, when $\lambda = \frac{2\pi}{k_x} >> 2a$, where a is the radius of the sphere and k_x the wavenumber in the direction of propagation.

The system considered is axially symmetric, so that the Laplacian can be written as

$$\nabla^2\phi(\mathrm{r},\omega) = \frac{1}{r^2}\frac{\partial}{\partial r}\left(r^2\frac{\partial\phi(\mathrm{r},\omega)}{\partial r}\right) + \frac{1}{r^2\sin\theta}\frac{\partial}{\partial\theta}\left(\sin\theta\frac{\partial\phi(\mathrm{r},\omega)}{\partial\theta}\right)\ , \tag{15}$$

where $\theta = 0$ is the direction of the polarisation of the incident electric field ($\hat{\mathbf{z}}$ in this case). Using separation of variables it can be demonstrated [14] that the solution of the Laplace equation has the general form

$$\phi(r,\theta,\omega) = \sum_{n=0}^{\infty}\left(A_n(\omega)r^n + B_n(\omega)r^{-(n+1)}\right)P_n(\cos\theta)\ , \tag{16}$$

for each domain, where $P_n(x)$ are Legendre polynomials. The electric field must be finite at all points. Therefore, inside the sphere the terms $r^{-(n+1)}$ are forbidden, since they lead to a divergence at $r = 0$. Furthermore, outside the sphere we do not include terms proportional to r^n when $n > 1$, because the associated electric field would diverge at infinity. Thus, the potential inside and outside the sphere have the general forms of

$$\phi_{\text{in}}(r,\theta,\omega) = \sum_{n=1}^{\infty}A_n(\omega)r^nP_n(\cos\theta)\ , \tag{17a}$$

$$\phi_{\text{out}}(r,\theta,\omega) = C_1(\omega)rP_1(\cos\theta) + \sum_{n=0}^{\infty}\left(D_n(\omega)r^{-(n+1)}\right)P_n(\cos\theta)\ . \tag{17b}$$

Note that no constant term is included since they do not have any effect on the electric fields.

We obtain the unknown constants (A_n, C_1 and D_n) by applying the boundary conditions. At infinity the contribution of the metallic particle is zero and only the incident electric field remains, $\phi_{\text{out}}(r \to \infty) = \phi_{\text{inc}}(r)$. Since $\phi_{\text{out}}(r \to \infty) = C_1 r P_1(\cos\theta)$, $\phi_{\text{inc}}(r) = -E_0 r \cos\theta$, and $P_1(\cos\theta) = \cos\theta$ we obtain that $C_1 = -E_0$. The boundary conditions in spherical coordinates are written as

$$\begin{aligned} \varepsilon_{\text{in}} E^r_{\text{in}}(r=a) = \varepsilon_{\text{out}} E^r_{\text{out}}(r=a) \quad &\longrightarrow \quad \varepsilon_{\text{in}} \frac{\partial \phi_{\text{in}}}{\partial r}\bigg|_{r=a} = \varepsilon_{\text{out}} \frac{\partial \phi_{\text{out}}}{\partial r}\bigg|_{r=a} , \\ E^\theta_{\text{in}}(r=a) = E^\theta_{\text{out}}(r=a) \quad &\longrightarrow \quad \frac{1}{a}\frac{\partial \phi_{\text{in}}}{\partial \theta}\bigg|_{r=a} = \frac{1}{a}\frac{\partial \phi_{\text{out}}}{\partial \theta}\bigg|_{r=a} . \end{aligned} \tag{18}$$

Since the Legendre polynomials are orthogonal, the potentials can be compared term by term. We then obtain that only A_0, A_1 and D_1 are not equal to zero. The final results is that the potential inside and outside the sphere are given by

$$\phi_{\text{in}}(r,\theta,\omega) = -\frac{3\varepsilon_{r,\text{out}}}{\varepsilon_{r,\text{in}}(\omega) + 2\varepsilon_{r,\text{out}}} E_0 r \cos\theta , \tag{19a}$$

$$\phi_{r,\text{out}}(r,\theta,\omega) = -E_0 r \cos\theta + \frac{\varepsilon_{r,\text{in}}(\omega) - \varepsilon_{r,\text{out}}}{\varepsilon_{r,\text{in}}(\omega) + 2\varepsilon_{r,\text{out}}} E_0 a^3 \frac{\cos\theta}{r^2} . \tag{19b}$$

The second term in equation 19b corresponds to a potential created by a quasi-static dipole,

$$\phi_{\text{out}}(\mathbf{r},\omega) = -E_0 r\cos\theta + \frac{\mathbf{p}_{\text{q}}(\omega)\cdot\mathbf{r}}{4\pi\varepsilon_{\text{out}} r^3} , \tag{20}$$

where the dipole moment is

$$\mathbf{p}_{\text{q}}(\omega) = 4\pi\varepsilon_{\text{out}} a^3 \frac{\varepsilon_{r,\text{in}}(\omega) - \varepsilon_{r,\text{out}}}{\varepsilon_{r,\text{in}}(\omega) + 2\varepsilon_{r,\text{out}}} \mathbf{E}_0 . \tag{21}$$

Noting $\mathbf{E}(\mathbf{r}) = -\nabla\phi(\mathbf{r})$ the electric field can be written as

$$\mathbf{E}_{\text{in}}(\mathbf{r},\omega) = \frac{3\varepsilon_{r,\text{out}}}{\varepsilon_{r,\text{in}}(\omega) + 2\varepsilon_{r,\text{out}}} \mathbf{E}_0 , \tag{22a}$$

$$\mathbf{E}_{\text{out}}(\mathbf{r},\omega) = \mathbf{E}_0 + \frac{3\hat{\mathbf{r}}(\hat{\mathbf{r}}\cdot\mathbf{p}_{\text{q}}(\omega)) - \mathbf{p}_{\text{q}}(\omega)}{4\pi\varepsilon_{\text{out}} r^3} . \tag{22b}$$

Equation 22a shows that the field inside the sphere is constant. On the other hand, The field outside the sphere (equation 22b) is given by two contributions, the constant excitation $\mathbf{E}_0$ and a scattered field which is induced due to the interaction between the nanosphere and the incident field.

Using the dipolar moment of the sphere (equation 21) the polarisability, defined as $\mathbf{p}_{\text{q}}(\omega) = \alpha(\omega)\mathbf{E}_0$, can be obtained

$$\alpha(\omega) = 4\pi a^3 \varepsilon_{\text{out}} \frac{\varepsilon_{r,\text{in}}(\omega) - \varepsilon_{r,\text{out}}}{\varepsilon_{r,\text{in}}(\omega) + 2\varepsilon_{r,\text{out}}} . \tag{23}$$

From this polarisability, the scattering and absorption cross sections can be calculated, which indicate how much light the sphere scatters and absorbs respectively. The sum of

these two cross sections is called extinction cross section. In the quasi-static approximation they can be written as [10]

$$\sigma_{sca}(\omega) = \frac{k^4}{6\pi\varepsilon_0^2}|\alpha(\omega)|^2 \,, \quad \sigma_{abs}(\omega) = \frac{k}{\varepsilon_0}\,\mathrm{Im}(\alpha(\omega)) \,, \quad \sigma_{ext}(\omega) = \sigma_{sca}(\omega) + \sigma_{abs}(\omega) \,. \quad (24)$$

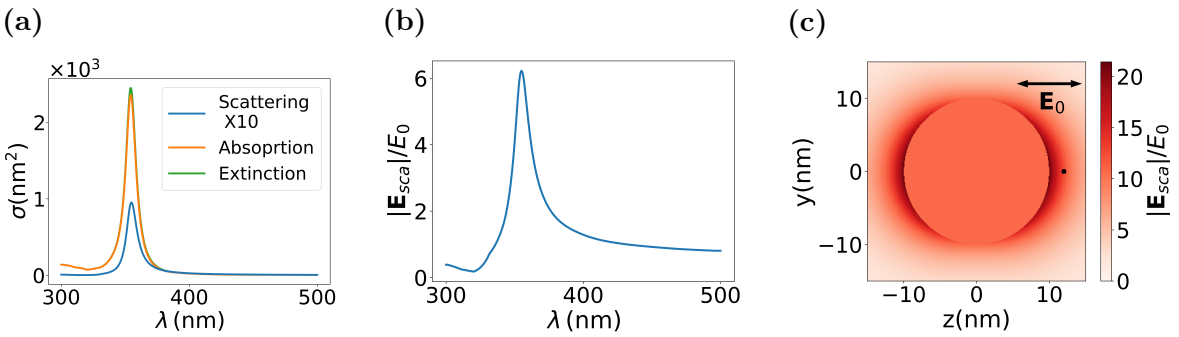

Figure 1: Optical response of a 10 nm radius sphere of silver surrounded by air, obtained using the quasi-static approximation and the experimental silver permittivity [12]. (a) Scattering multiplied by ten (blue line), absorption (orange line) and extinction (green line) cross sections spectra. (b) Electric field enhancement at a position situated 2 nm away from the surface of the sphere in the direction of the incident field. (c) Normalised electric field distribution at the plane x=0 for resonant illumination. The polarisation of the incident electric field is represented by the black arrow. The black point represents the position where the electric field is evaluated in (b).

The electric field and the cross sections present a resonance when the polarisability is maximum, that is when $\varepsilon_{r,\mathrm{in}}(\omega) \approx -2\,\mathrm{Re}(\varepsilon_{r,\mathrm{out}})$. This resonance corresponds to the plasmon. In figure 1a we show the cross sections for a 10 nm silver sphere in the quasi-static approximation, where we see a clear resonance at wavelength $\lambda = 355$ nm. It is also interesting to analyse how the electric field is enhanced near the nanosphere. Figure 1b shows the field enhancement spectra at 2 nm from the surface of the sphere in the direction of the polarisation of the incident field. We can observe a clear peak in the field spectra at the same wavelength as the resonances in the cross sections. We show on the figure 1c the field distribution of the absolute value of the scattered field. The electric field outside the sphere follows a dipolar pattern, whereas inside it is constant.

The resonances that can be excited in plasmonics structures are quite broad, as shown in figure 1. The width of the resonances is strongly influenced by the losses of the system, that is, by the imaginary part of the permittivity of the metal, smaller losses leading to narrower resonances. On the other hand, the field enhancement of a silver nanosphere is of the order of 10, which can be increased significantly by changing the shape of the nanostructure, for example by using structures with nanometric gaps (subsection 4.1). Last, the field distribution near the sphere (figure 1c) demonstrates that the plasmonic structures are able to localise light into the nanometric regime, surpassing the diffraction limit.

3 Introduction to the Finite element method (FEM)

Analytical solutions are limited only to a few structures, so that computational methods are often needed, such as based on the finite element method (FEM). We use a commercial FEM simulator (COMSOL multiphysics [15]), but we present a short introduction to FEM below to understand its main principles.

3.1 Basic principles

Instead of focusing on how FEM is applied to solve Maxwell's equations, which is quite complex, we analyse the case of a simple differential equation in one dimension. To achieve a basic understanding of the formalism, we consider the following equation:

$$u''(x) = f(x) \quad x \in [0,1] \qquad \text{(25a)} \qquad u(0) = 0, \quad u(L) = 0\ . \qquad \text{(25b)}$$

The first step for FEM is to get the variational formulation of our equation, also called the weak form. This formulation is a equivalent equation which is obtained by multiplying the two sides of equation 25a with a prove equation $v(x)$ and taking the integral [16],

$$\int_0^L u''(x)v(x)\mathrm{d}x = \int_0^L f(x)v(x)\mathrm{d}x\ . \tag{26}$$

Implementing integration by parts and assuming that the prove function has the same boundary conditions as the $u(x)$ function the equation can be rewritten as

$$\int_0^L f(x)v(x)\mathrm{d}x = u'(x)v(x)\Big|_0^L + \int_0^L u'(x)v'(x)\mathrm{d}x = \int_0^L u'(x)v'(x)\mathrm{d}x\ . \tag{27}$$

In order to resolve this equation computationally the space is discretised in small regions and the function u(x) is expressed as a linear combination of a specific basis $\psi_i(x)$, $u(x) = \sum u_i\psi_i(x)$. In this expansion, u_i are the weight factors of each function of the basis and their values need to be determined. For example, a basis used by COMSOL is a group of triangle functions which each one is unity at the centre of its discretisation point and zero a the points of the following discretisation [17]. Since equation 26 must be verified for any function it has to be also fulfilled when $v(x)$ is any basis function $\psi_j(x)$. Expressing $u(x)$ in the $\psi_i(x)$ basis we get the following equation for each j:

$$\sum_i u_i \int_0^L \psi_i'(x)\psi_j'(x)\mathrm{d}x = \int_0^L f(x)\psi_j(x)\mathrm{d}x\ . \tag{28}$$

This equation can be written in matrix form as

$$Au = b\ , \tag{29}$$

where the unknown coefficient (u_i) are the elements of the vector u. Finally, this equation can be solved with any matrix solver.

Maxwell's equations are more complicated than the example explained above in the following ways. First, because the systems are three dimensional, the equations need to

be generalised to 3D e.g. using gradients instead of derivatives. Further, plasmonic structures are open systems, that is, they extend to infinity. Since infinite space cannot be discretised, perfectly matched layers (PMLs) are used. The PMLs surround all the system and are essentially forced boundary conditions that absorb all the electromagnetic fields that propagate to them. Additionally, the boundary condition of Maxwell's equations are more complex than the simple boundary conditions (equation 25b) analysed above.

3.2 Optical response of a nanosphere

We calculate the response of a silver sphere using COMSOL and compare it to the results obtained theoretically via the quasi-static approximation (subsection 2.3.1). First, we need to specify the geometry and the permittivities of the materials in COMSOL (including PMLs). We use again experimental values of the silver permittivity [12]. After defining the system, COMSOL calculates the induced field distribution, which can be used to calculate the scattering and absorption cross sections. The scattering cross section is obtained by integrating over an enclosed surface the component of the Poynting vector of the scattered field that is normal to this surface. Similarly, the absorption cross section is calculated as the volume integral of the power loss density in the nanoparticle. Critically, for each system, a convergence study is needed (appendix A) to ensure that the results do not change if better spatial discretisation is used (better mesh) and if the PMLs are situated further away from the object (larger simulation region).

The symmetry of the system allows for decreasing the matrix size and thus reducing the computational time. The system considered has two plane symmetries parallel to the direction of the incoming electromagnetic wave. For example, in our case the wave propagates in the x direction, therefore the planes of symmetry are xz and xy. Thus, it is possible to reduce the number of discretisation cells and in consequence the matrix size four times.

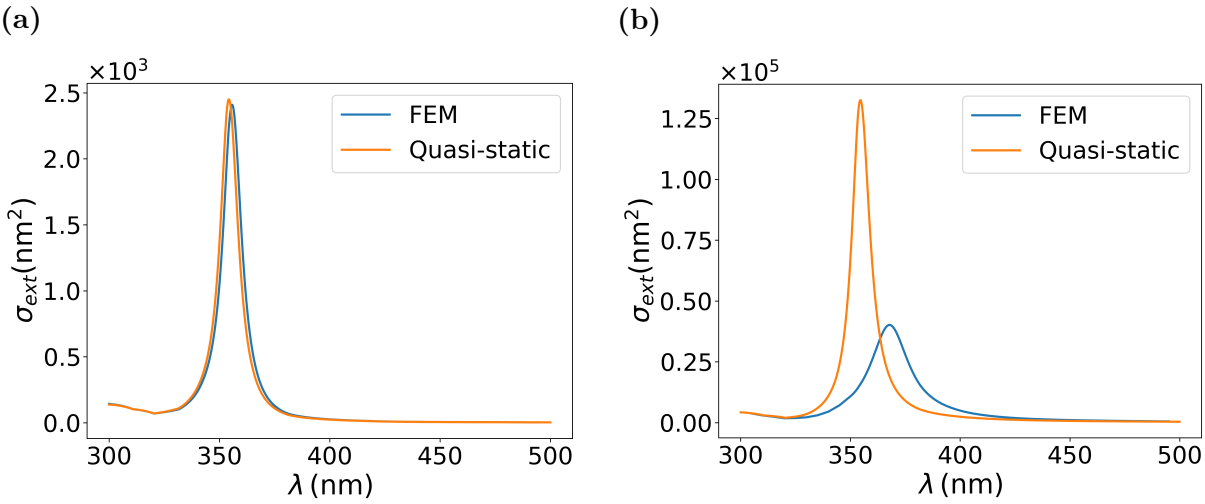

Figure 2: Comparison between the extinction cross section using the quasi-static approximation (orange line) and FEM results (blue line) for a silver sphere surrounded by air. Extinction cross sections (a) for the 10 nm-radius sphere and (b) for the 30 nm-radius sphere.

Figure 2a shows the quasi-static extinction cross section (orange line) and the extinction cross section obtained with FEM (blue line) for a 10 nm sphere. To ensure that the FEM results are correct, we compared them with the analytical exact solutions (not shown) that were obtained using a free Mie program [18]. We can observe that the differences between the FEM and quasi-static results are very small. On the other hand, we show in figure 2b the same comparison for a 30 nm radius sphere. In this case, the two results are quite different from each other. The resonance in the extinction cross section obtained using FEM (blue line) is less strong and broader and the peak is found at larger wavelengths (the resonance redshifts). Although in the quasi-static approximation the position of the resonances does not depend on the size of the sphere, in reality increasing the size red-shifts the resonances. Further, we conclude that quasi-static approximation gives important information about plasmonic systems, but computational results are needed for spheres larger than ≈ 20 nm.

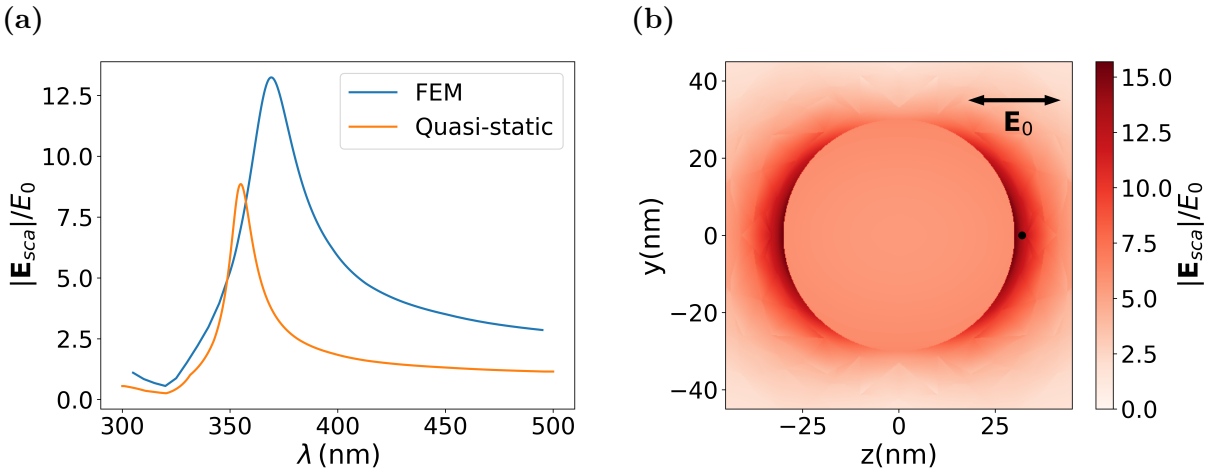

Figure 3: Fields induced of a 30 nm radius sphere of silver surrounded by air illuminated by a plane wave propagating in x direction and polarised in z direction. (a) Field enhancement spectra at 2 nm from the surface of the sphere along the direction of polarisation (black dot in (b)). The blue line is calculated with FEM simulations whereas the orange line represents the quasi-static result. (b) Spatial distribution of the field near the sphere calculated using FEM. The black arrow indicates the polarisation of the incident electric field.

Further, the field enhancement spectra calculated with FEM for a 30 nm radius sphere (blue line in figure 3a) is also different from the one given by the quasi-static approximation (orange line in figure 3a), The FEM result shows a broader resonance characterised by stronger field enhancement. Last, Figure 3b shows a map of the scattered field near the nanosphere calculated using FEM. We observe that the field inside the sphere is constant and outside it has a dipolar pattern, in a similar way as for the quasi-static results, which indicates that we are exciting the dipolar mode.

4 Nanoparticle on a mirror (NPoM)

In the previous chapters, we have focused on the case of a simple sphere to illustrate the properties of plasmonic resonances. This simple sphere allows achieving field enhancements of the order of 10. However, for practical applications, it is convenient to increase this field enhancement as much as possible. A convenient approach is to use nanometric gaps between two metallic structures. We specifically focus on a nanoparticle on a mirror (NPoM), which is formed by a metallic nanoparticle placed in a metallic substrate with a nanometric (≈ 1 nm) gap between them (figure 4c). This structure enables to achieve bigger field enhancements than 100 in the gap. The physical principles behind the optical response of the NPoM and of two metallic spherical nanoparticles are very similar. Thus, before discussing the NPoM in subsection 4.2, we first explain how the two sphere system responds to an incident plane wave.

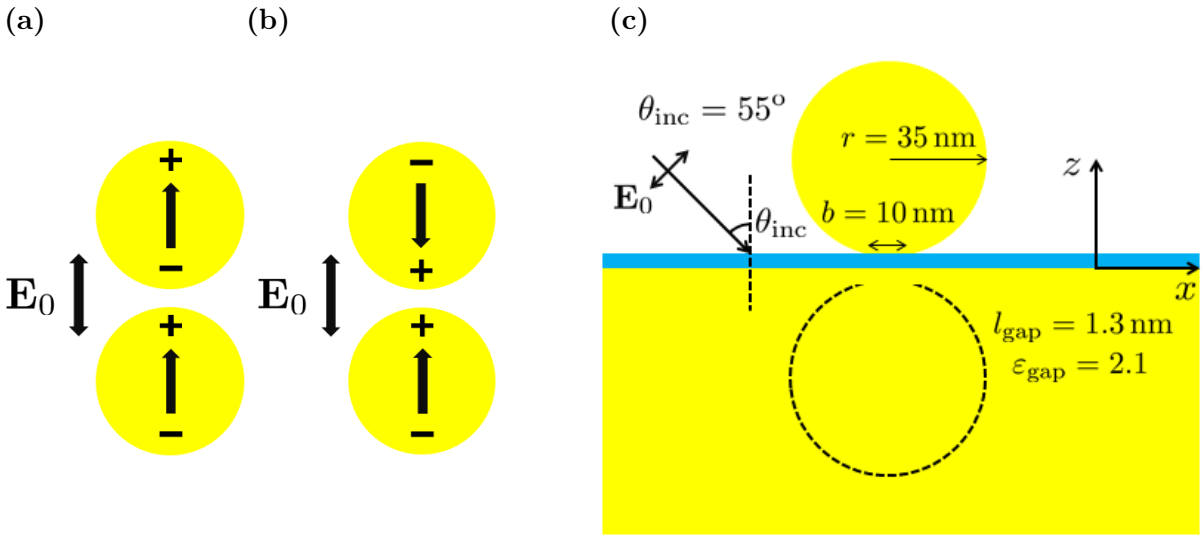

Figure 4: Sketch of the (a) bonding and (b) antibonding dimer plasmon for two spheres in air. The arrows inside the spheres indicate the direction of the induced dipoles, and the plus and minus signs the charge distribution (at a given time). The black arrow outside the sphere correspond to the direction of polarisation of the exciting field $\mathbf{E}_0$. (c) Sketch of the nanoparticle on a mirror (NPoM). The NPoM consists in a metallic sphere deposited in an infinite metallic substrate with a nanometric dielectric gap (representing a molecular monolayer) between them. The sphere present a flat facet at the bottom (region of contact with the molecules). The sphere marked with dashed lines represents the virtual image produced by the reflection of the upper sphere on the substrate. The tilted arrow shows the propagation direction of the incident plane wave. It propagates in the xz plane at an θ_{inc} angle from the normal z to the substrate (see axis on the sketch). The field is polarised in the xz plane in the direction specified by the solid line (TM polarisation). As indicated in the figure, the radius of the sphere is $r = 35$ nm, the diameter of the flat facet of the sphere at the bottom is $b = 10$ nm, the size of the gap is $l_{\text{gap}} = 1.3$ nm and the permittivity of the gap is $\epsilon_{\text{gap}} = 2.1$. The system is surrounded by air.

4.1 Nanometric gaps between two metallic nanoparticles

When two small nanospheres are excited by a plane wave, each one can be described in a first approximation as a dipole pointing in the direction of the excitation. If they

are placed very close together, at nanometric distance, these two dipoles interact with each other, which lead to plasmonic hybridisation, and thus to the formation of two new hybrid modes, the bonding and antibonding dimer plasmon. This effect reminds the process of two interacting molecules, which give rise to two new energy states, the bonding and antibonding orbitals. In the case of the bonding dimer plasmon the dipoles point in the same direction (figure 4a), which decreases the energy of this hybrid mode. Thus, the dipolar resonance is redshifted in comparison with the result for one sphere [19]. Additionally, the illumination induces positive charges on the surface near the gap of one sphere (at a given time) and negative charges on the other sphere. Since these charge distributions are separated only by few nanometers or less, very large electric fields are induced in the gap. The smaller is the gap the bigger is the field induced until, for gaps around 0.5 nm or smaller, quantum tunnelling effects arise, reducing the charge density and therefore the field enhancement. On the other hand, in the antibonding plasmon the induced dipoles point in the opposite direction (figure 4b), which increases the energy of the system blueshifting the resonance. In this configuration, the two spheres have positive or negative charges near the gap, so they do not induce such large fields as in the bonding configuration. Further, the antibonding resonance is difficult to excite in practical situations, so that we focus on the bonding dimer plasmon in this work.

Unfortunately, it is not easy to fabricate two nanospheres separated by a nanometric gap between them. Furthermore, it is very interesting to deposit molecules in this gap and characterise them using the big field enhancements achieved. The process of placing molecules between the spheres is also quite arduous. An alternative to achieve similar physical behaviour consist of a metallic nanoparticle placed on a metallic substrate with a small gap between them, called nanoparticle on a mirror (NPoM). The substrate produces a virtual image of the charge distribution of the nanoparticle, that is, the substrate can act as a mirror that reflects the charges. The NPoM can be fabricated relatively easy. First, a thin layer of molecules is placed in the substrate and then the nanosphere is deposited over this layer. This fabrication process automatically places the molecules at the gap, i.e. at the position of strong field enhancement, as desired.

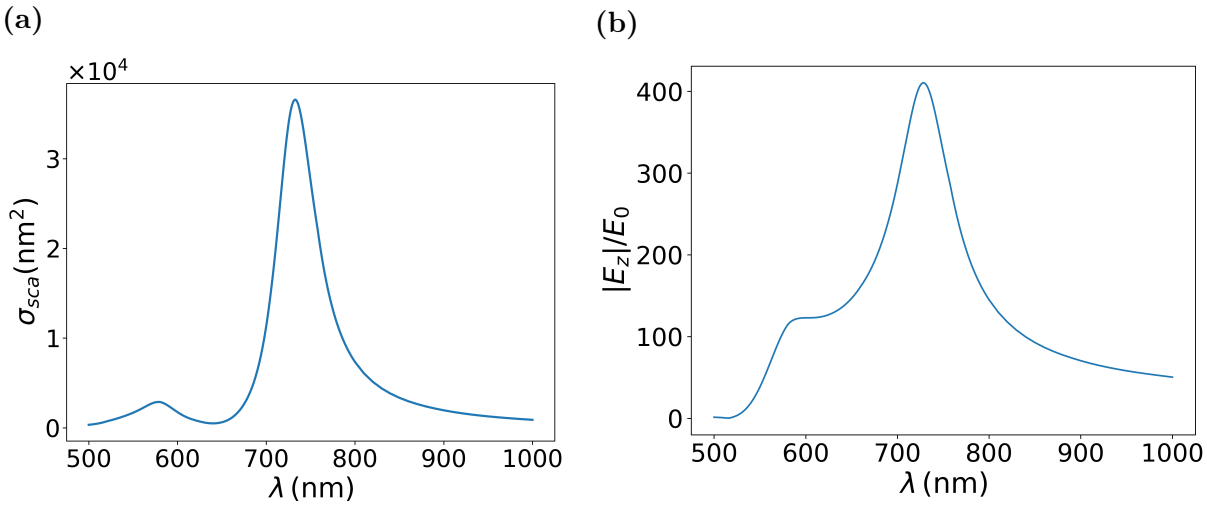

Figure 5: (a) Scattering cross section and (b) spectra of the z component of the field enhancement ($|E_z|/E_0$) in the middle of the gap calculated with FEM for the nanoparticle on a mirror sketched in figure 4c.

4.2 FEM results of the optical response of a NPoM

In the work, we study a specific NPoM formed by a 35 nm radius gold sphere with a 10 nm diameter flat facet surrounded by air. The gap between the spherical particle and the infinite gold substrate is $l_{\text{gap}} = 1.3$ nm and the molecules placed on it are described by an effective dielectric layer with $\varepsilon_{\text{gap}} = 2.1$. The flat facet is found at the interface with the molecules. The use of a flat facet next to the gap instead of using a perfect sphere allows to be closer to the experimental situation and to interact with more molecules at the gap. The system is excited by a transverse magnetic (TM) plane wave (as illustrated in figure 4c) that propagates at an angle of $\theta_{\text{inc}} = 55^{\text{o}}$ with respect to the normal of the substrate. In TM polarisation the electric field is polarised parallel to the plane of propagation (in this case the xz plane). The amplitude of the electric field is E_0. As a technical note, to obtain the response of this system with COMSOL, it is convenient to first obtain the analytical solution of the same system but without the spherical nanoparticle. This solution is discussed in appendix B. Further, the system is symmetric with respect to plane xz, so that it is possible to consider only half of the structure in the numerical calculations.

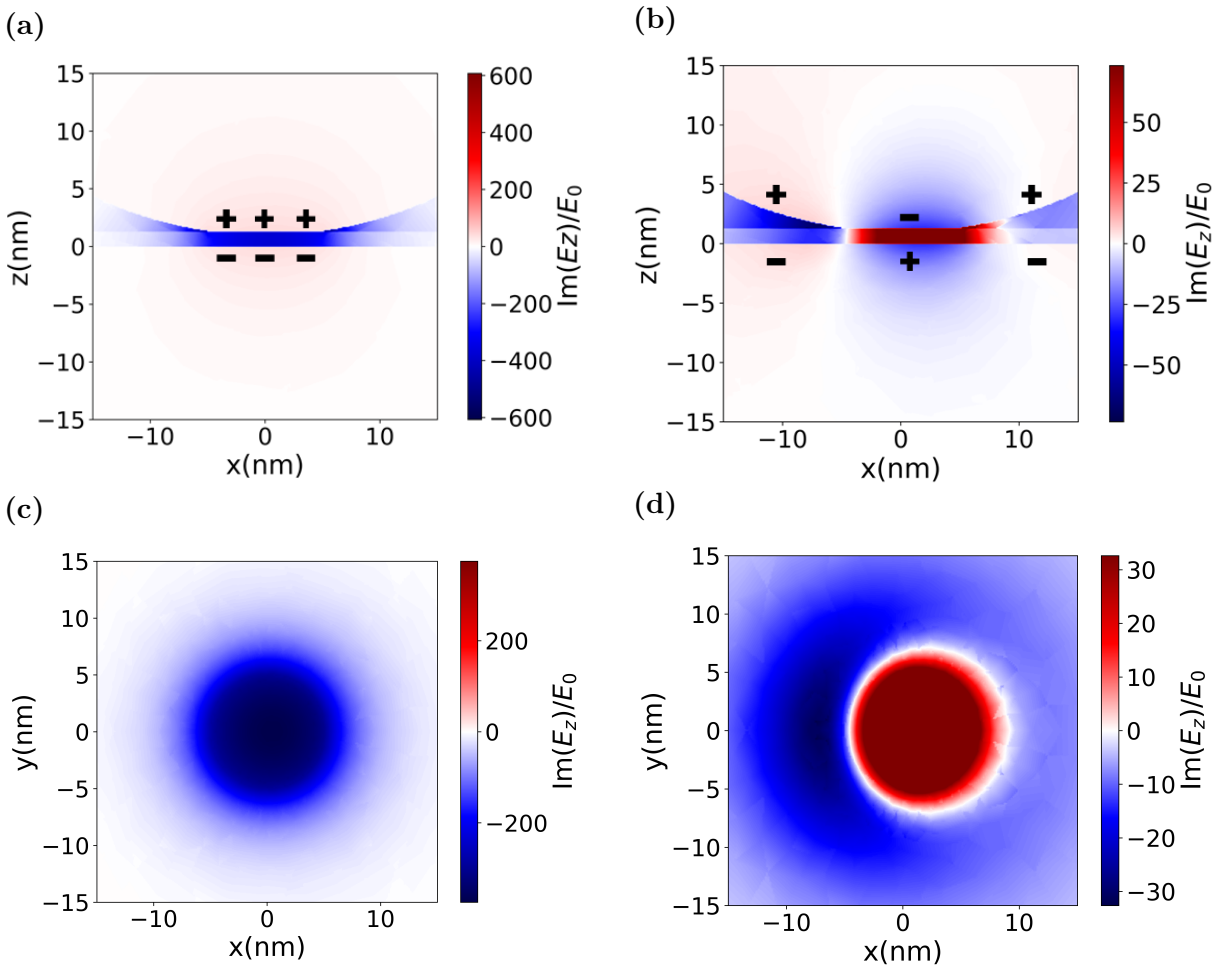

Figure 6: Distribution of the imaginary part of the scattered electric field near the gap for the same NPoM as in figure 4c. (a) and (b) correspond to the field at the y=0 plane for 730 nm and 580 nm illumination wavelength, respectively. The plus and minus signs represents schematically the resulting charge distributions. (c) and (d) are the equivalent results as in (a) and (b), but at the horizontal xy plane crossing the middle of the gap.

We show in figure 5a the scattering cross section of this NPoM and in figure 5b the z component of the field enhancement at the middle of the gap. In both figures we observe two maximums, a very clear one at 730 nm wavelength and a weaker one at 580 nm. These maxima correspond to the resonances of the system. Comparing the results of the NPoM with the results for a single sphere (figure 3a), we find that nanometric gaps enable to increase the field enhancement near the nanoparticle more than for the single sphere, reaching values of the order of 400 for the NPoM.

To analyse the resonances it is very useful to calculate the field distributions of the electric fields in the gap at the wavelengths (λ) of the corresponding maxima. In figure 6a and 6c we plot the field distributions in the xz and xy planes at $\lambda = 730$ nm. We observe that the field in the gap is approximately constant in the z direction and that it is very large. At a given time, the induced charges at the gap region are negative in the metallic substrate and positive in the bottom flat facet of the nanoparticle (figure 6a) because the field is pointing in the negative z direction (negative values of E_z). Further, although we do not show here, at the top of the sphere negative charges are induced. These charge densities indicate that we are exciting the bonding dipolar mode. On the other hand, we show in figures 6b and 6d the field distribution in the xz and xy planes at $\lambda = 580$ nm, corresponding to the second plasmonic resonance which is characterised by a weaker field enhancement. The field distribution is more complex in this case. It presents fast changes in the gap that result in multiple changes of the sign of the charge distribution at a given time: positive-negative-positive charge distribution on the bottom of the nanoparticle and negative-positive-negative charges on the substrate (figure 6b). In addition, on the top of the nanoparticle negative charges are again induced. Thus, the resonances at $\lambda = 580$ nm are due to the bonding quadrupolar mode.

5 Quasinormal mode (QNM) formalism

The FEM simulations in subsections 3.2 and 4.2 give directly the near-filed and cross section spectra for a given illumination and the identification of the modes require additional effort. Recently, a quasinormal modes formalism has been developed in order to better understand the plasmonic response of a system and in some cases to improve the computational time. The main idea of this new method is to resolve Maxwell's equations in frequency domain without any excitation. Therefore, the problem is transformed to an eigenvalue (ω_n) and eigenfunction ($\mathbf{E}_n(\mathbf{r})$ and $\mathbf{B}_n(\mathbf{r})$) problem. The eigenfunctions of the system are the quasinormal modes. They are called quasinormal modes and not simply modes because the plasmonic structures has losses and therefore the Hamiltonian is not Hermitian. In consequence, the eigenvalues are complex numbers. We obtain the eigenvalue problem from Maxwell's equations,

$$\begin{bmatrix} 0 & \frac{i}{\varepsilon_0\varepsilon_r(\omega_n)\mu_0}\nabla\times \\ -i\nabla\times & 0 \end{bmatrix} \begin{bmatrix} \mathbf{E}_n(\mathbf{r}) \\ \mathbf{B}_n(\mathbf{r}) \end{bmatrix} = \omega_n \begin{bmatrix} \mathbf{E}_n(\mathbf{r}) \\ \mathbf{B}_n(\mathbf{r}) \end{bmatrix} . \tag{30}$$

With equation 30 we calculate the quasinormal modes of the field without introducing any external excitation, which for example can be done using a FEM simulator (COMSOL in our case). For the following it is important to distinguish between the direct FEM simulations of the response of the system that we have discussed in subsections 3.2 and 4.2 and the FEM simulations used to resolve the eigenvalue problem of equation 30. For simplicity, we would refer to them as the FEM and QNM calculations, respectively.

After computing the QNMs of the system, we calculate the electromagnetic response for a specific external excitation. The scattered field can be written as a linear combination of the QNMs [7],

$$\begin{bmatrix} \mathbf{E}_{\text{sca}}(\mathbf{r},\omega) \\ \mathbf{B}_{\text{sca}}(\mathbf{r},\omega) \end{bmatrix} = \sum_n \alpha_n(\omega) \begin{bmatrix} \mathbf{E}_n(\mathbf{r}) \\ \mathbf{B}_n(\mathbf{r}) \end{bmatrix} , \tag{31}$$

where α_n are the modal coefficients. The value of these coefficients, where the illumination is introduced, is given by the closed expression that we discuss in subsection 5.1. A non-zero value of a modal coefficient indicates that the corresponding mode of the system is excited by the incident electromagnetic wave. Thus, once the QNMs of the system are known (which do not depend on the excitation), we only need to calculate the modal coefficient for a specific illumination and expand the scattered fields in terms of the QNMs according to equation 31. Computationally it is much faster to calculate the modal coefficients than to solve Maxwell's equations. Therefore, once the quasinormal modes are calculated, the QNM formalism is more efficient than FEM simulations.

Importantly, in order to express the scattered fields as a linear combination of the QNMs, the eigenfunctions must be normalised. The normalisation is obtained by integrating into all space the dot product of the eigenfunctions, $\mathbf{E}_n \cdot \mathbf{E}_n$. However, plasmonic systems are open systems and the integral diverges, and therefore the normalisation also diverges. To work with these divergences different techniques have been developed. For instance, in an initial approach, the eigenfunctions were only normalised inside the nanoparticle getting a finite normalisation constant [8]. Nevertheless, this has the drawback that the modes constitute a complete set only inside the resonant structure and not outside the particle, although the fields outside the plasmonic particles are typically also

very important. In this work, we use the method developed by Phillipe Lalanne and its group [20], where perfectly matched layers (PMLs) are used to limit the infinite space. In this way, the modes form a complete set in all space, although a disadvantage is that some modes appear that are not the real modes of the plasmonic structure, called PML modes. To get an exact solution, these PML modes must be taken into account, which complicates the analysis as discussed below.

5.1 QNMs using auxiliary fields

To obtain the normalisation of the QNMs we need an analytical expression of the permittivity to describe the dispersive materials for complex frequencies. We specifically use the Drude-Lorentz permittivity given by equation 13. Further, if we define as auxiliary fields the polarisation and current components ($\mathbf{P}_i$ and $\mathbf{J}_i$) we obtain

$$\mathbf{P} = -\varepsilon_0\varepsilon_\infty \sum_{i=1}^{N} \frac{\omega_{p,i}^2}{\omega^2 - \omega_{0,i}^2 + i\gamma_i\omega}\mathbf{E} = \sum_{i=1}^{N}\mathbf{P}_i \quad \text{and} \quad \mathbf{J} = -i\omega\mathbf{P} = \sum_{i=1}^{N}\mathbf{J}_i \,, \tag{32}$$

which are the polarisation and the current respectively. Here, in the sum of the Lorentzians, the i=1 term corresponds to the Drude term ($\omega_{0,1} = 0$). Introducing the Drude-Lorentz permittivity (with only one Lorentz term for simplicity, i.e. the Drude term) and the auxiliary fields in equation 30, we can obtain four linear differential equations:

$$\begin{aligned}
&1)\ \frac{1}{\varepsilon_0\mu_0\epsilon_r}\nabla\times\mathbf{B} = \omega\mathbf{E} \quad \longrightarrow \quad \frac{1}{\varepsilon_0\mu_0\epsilon_\infty}\nabla\times\mathbf{B} - \frac{i}{\varepsilon_0\varepsilon_\infty}\mathbf{J}_i = \omega\mathbf{E} \\
&2)\ -i\nabla\times\mathbf{E} = \omega\mathbf{B} \qquad\qquad 3)\ i\mathbf{J}_i = \omega\mathbf{P}_i \\
&4)\ \mathbf{P}_i = -\varepsilon_0\varepsilon_\infty\frac{\omega_{p,i}}{\omega^2-\omega_{0,i}^2}\mathbf{E} \quad \longrightarrow \quad i\varepsilon_0\varepsilon_\infty\omega_{p,i}^2\mathbf{E} - i\omega_{0,i}^2\mathbf{P}_i - i\gamma_i\mathbf{J}_i = \omega\mathbf{J}_i
\end{aligned} \tag{33}$$

We can then, write these equations in matrix form as

$$\begin{bmatrix} 0 & \frac{i}{\mu_0\varepsilon_0\varepsilon_\infty}\nabla\times & 0 & -\frac{i}{\varepsilon_0\varepsilon_\infty} \\ -i\nabla\times & 0 & 0 & 0 \\ 0 & 0 & 0 & i \\ i\varepsilon_0\varepsilon_\infty\omega_p^2 & 0 & -i\omega_0^2 & -i\gamma \end{bmatrix} \begin{bmatrix} \mathbf{E}_n \\ \mathbf{B}_n \\ \mathbf{P}_n \\ \mathbf{J}_n \end{bmatrix} = \omega_n \begin{bmatrix} \mathbf{E}_n \\ \mathbf{B}_n \\ \mathbf{P}_n \\ \mathbf{J}_n \end{bmatrix} \,, \tag{34}$$

which is lineal and must be solved to calculate the quasinormal modes. In section 6 we use two Lorentz terms instead of only one, so that the size of the matrix in the left of equation 34 is 6x6 (in reality 18x18 since the eigenfunctions are vectors). On the other hand if the material does not depend on the frequency it is enough to consider equation 30.

All the quasinormal modes are orthogonal, including modes associated with the PMLs. To normalise the solutions of equation 34 we need a normalisation factor A_n, which is calculated from the orthogonality relation between the modes,

$$\begin{aligned}
\frac{1}{A_n^2}\int_V \Bigg(&\varepsilon_0\varepsilon_\infty\mathbf{E}_n\cdot\mathbf{E}_{n'} - \frac{1}{\mu_0}\mathbf{B}_n\cdot\mathbf{B}_{n'} \\
&+ \sum_{i=1}^{N}\frac{\omega_{0,i}^2}{\varepsilon_0\varepsilon_\infty\omega_{p,i}^2}\mathbf{P}_{n,i}\cdot\mathbf{P}_{n',i} - \sum_{i=1}^{N}\frac{1}{\varepsilon_0\varepsilon_\infty\omega_{p,i}^2}\mathbf{J}_{n,i}\cdot\mathbf{J}_{n',i}\Bigg)\mathrm{d}\mathbf{r} = \delta_{nn'} \,,
\end{aligned} \tag{35}$$

where the integral must be extended over all the system delimited by PMLs. $\delta_{n,n'}$ is the Kronecker delta, which is 1 when n and m are equal and 0 otherwise. If the material is not dispersive the polarisations and the currents are zero and, instead of ϵ_∞, ϵ_r should be used. From this equation we obtain the values of the normalisation constant A_n using $n' = n$.

It can be demonstrated [8] that the modal coefficients can then be written as

$$\alpha_n = \frac{1}{A_n} \frac{\varepsilon_0}{\omega_n - \omega} \left(\omega(\varepsilon_\infty - \varepsilon_b) - \omega_n(\varepsilon_\infty - \varepsilon_r(\omega_n))\right) \int_{V_{\text{res}}} \mathbf{E}_n \cdot \mathbf{E}_{\text{inc}} \mathrm{d}\mathbf{r} \ . \tag{36}$$

ε_b is the relative permittivity of the surrounding media and in contrast with the orthogonality relation, the overlapping integral between the incident electric field and the QNM needs to be calculated in the nanoparticle domain. Further, the expressions for the extinction and absorption cross section can be obtained,

$$\sigma_{\text{ext}} = -\frac{\varepsilon_0}{2I_0} \sum_n \text{Im}\left(\alpha_n(\omega(\varepsilon_\infty - \varepsilon_b) + \omega_n(\varepsilon_r(\omega_n) - \varepsilon_\infty)) \int_{V_{\text{res}}} \mathbf{E}_n \mathbf{E}^*_{\text{inc}} \mathrm{d}\mathbf{r}\right) \ , \tag{37a}$$

$$\sigma_{\text{abs}} = \frac{1}{2I_0} \sum_{i=1}^{N} \frac{\gamma_i}{\varepsilon_0 \varepsilon_\infty \omega_{p,i}^2} \int_{V_{\text{res}}} |\mathbf{J}_i|^2 \mathrm{d}\mathbf{r} \qquad \text{where} \qquad \mathbf{J}_i = \sum_n \alpha_n \mathbf{J}_{n,i} \ . \tag{37b}$$

I_0 is the intensity of the incident electromagnetic wave, $I_0 = \frac{1}{2} E_0^2 \sqrt{\frac{\varepsilon_0}{\mu_0}}$. To obtain the field distribution near the particles we only need to evaluate equation 31.

We calculate the quasinormal modes of the system using COMSOL multiphysics [15]. After that, using a Matlab program developed by the group of Philippe Lalanne [20] we obtain the cross sections and modal coefficients for a specific illumination.

5.2 Plasmonic nanosphere

To test the QNM calculations we analyse the case of a sphere of 30 nm radius surroundeed by air, and compare the results to FEM simulations of the same system. For the permittivity of the metal we use a simple Drude model,

$$\varepsilon_r(\omega) = \varepsilon_\infty \left(1 - \frac{\omega_p}{\omega^2 + i\gamma\omega}\right) \ , \tag{38}$$

$$\varepsilon_\infty = 1 \ , \quad \omega_p = 1.3659 \cdot 10^{16} \, \text{rad/s} \ , \quad \gamma = 0.0023\omega_p \ .$$

We show in figure 7a the QNMs of the plasmonic structure (red dots), which due to the spherical symmetry of the system are degenerate: the first mode is three times degenerate, the second one five times... In the figure, the x-axis give the resonant frequency ($\text{Re}(\omega_n)$) and the y axis indicates the losses ($\propto \text{Im}(\omega_n)$). Furthermore, in addition to the modes of the structure, other modes appear (blue dots), which are called PML modes. These modes are the consequence of limiting the infinite space with the perfectly matched layers (PMLs), so that we are not simulating only the spherical particle. We can differentiate the PML modes from the main modes of the structure because PML modes change when the

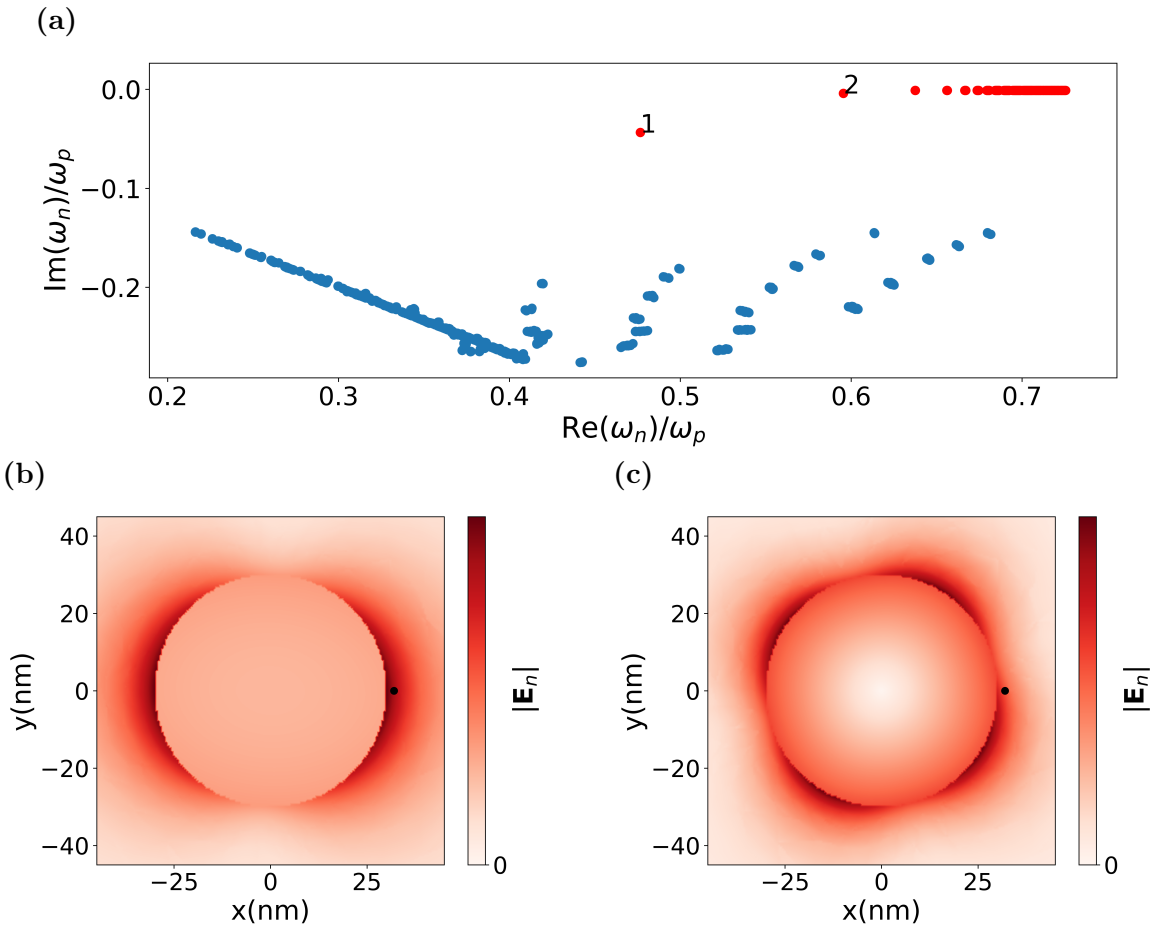

Figure 7: (a) 2000 quasinormal modes of a 30 nm radius metallic sphere (the permittivity is given by equation 38) surrounded by air. The red dots are the real modes of the plasmonic structure and the blue dots are the PML modes. The number 1 and 2 indicate the first (lowest in energy) and the second order modes of the structure. (b,c) Map of the electric field amplitude $|\mathbf{E}_n|$ for (b) the first order mode and (c) the second order mode. The black point represents the position where the field enhancement is evaluated in figure 9.

parameters of the perfectly matched layers are changed. To obtain the electromagnetic result of the system these PML modes must also be taken into account.

A big advantage of the QNM formalism is that we obtain directly the plasmonic modes, in contrast with the FEM simulations. In the latter case, we calculate the full spectra and it is not always straightforward to distinguish the contribution of each mode, especially when the resonances are very near from each other. In figures 7b and 7c we show the field distributions ($|\mathbf{E}_n|$) of the first (lowest in energy) and second order QNMs respectively. From these field distributions, we can conclude that the first QNM is a dipolar mode and the second one a quadrupolar mode. Further, we show in figure 8 the total extinction cross section of the system calculated with the QNM formalism (dashed red line) and the contribution of the first three quasinormal modes corresponding to the dipolar mode (blue line), quadrupolar mode (orange line) and octopolar mode (green line). The QNM formalism is thus a suitable method to distinguish the contribution from each mode. Further, we observe that by only taking the three modes that contribute the most to the electromagnetic response we can represent very well the total result. Being able to

describe the response with only a few resonances is very useful, for example, to develop analytical models.

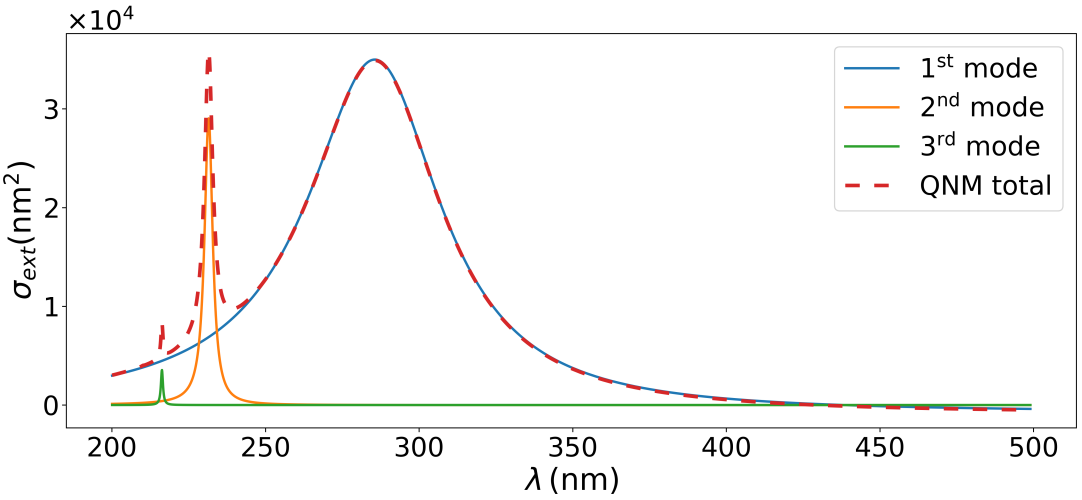

Figure 8: Extinction cross section obtained using the QNM formalism for the 30 nm radius sphere (the permittivity is given by equation 38) surrounded by air for plane wave illumination. We separate the contribution of the first (blue line), second (orange line) and third (green line) order modes to the total extinction cross section (dashed red line).

We show in figures 9 the comparison between the QNM results (orange lines) and the corresponding FEM spectra (blue lines). We have found that it is significantly harder to obtain a good convergence for QNM simulations than for FEM calculations, requiring a better discretisation (see appendix A for further discussion). Figure 9a shows that the extinction cross sections calculated with FEM and the QNM formalism are very similar near the resonant peaks. We observe some appreciable discrepancies at small and large wavelengths (at large values the extinction reaches small negative values when using QNMs, which is unphysical). However, notice that the scale of the vertical axis is logarithmic, so that the differences appear when the extinction is very small. Further, we show in figure 9b the enhancement spectra of the z component of the electric field ($|E_z|/E_0$) at 2 nm from the surface of the sphere (at the position marked by a black dot in figures 7b and 7c). We observe a similar behaviour as in the extinction cross section. The resonances are very well described by the QNM results, but at high wavelengths, some differences become visible. However, in the case of the field enhancement, the relative error between the QNM and FEM results is smaller than for the extinction cross section.

The results in figure 9 indicate that the QNM formalism is able to describe the main features of the spectra and that the differences between QNM and FEM results are relatively small. However, it is important to analyse what is the source of these differences and try to improve the agreement. We believe that the differences are because we are not taking all the quasinormal modes into account due to computational limitations. We are including in equation 37a all quasinormal modes in figure 7a, but this calculation does not include enough modes, especially the PML modes. In the next subsection, to be able to calculate more modes, we reduce the system to 2D calculations, which are significantly more efficient than the 3D simulations considered in this subsection.

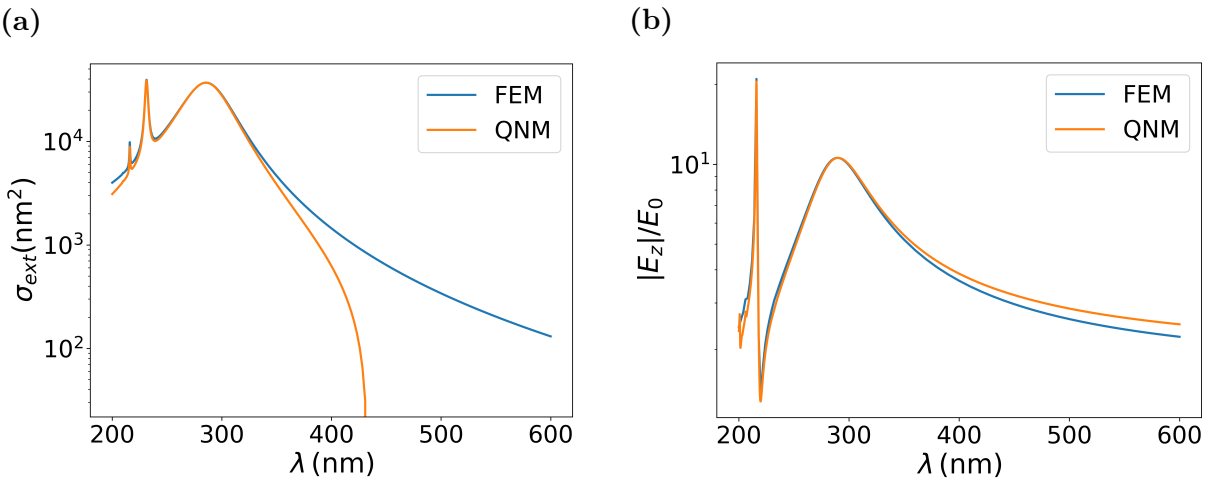

Figure 9: Comparison between FEM results (blue lines) and QNM results (orange lines) for a 30 nm radius sphere (the permittivity is given by equation 38) surrounded by air using a z polarised plane wave as excitation. (a) Extinction cross section and (b) z component of the field enhancement ($|E_z|/E_0$) at 2 nm away from the surface (z=32 nm). The y axis in both panels is in logarithmic scale to show more clearly the differences between QNM and FEM results.

5.3 Implementation of the QNM formalism for axially symmetric systems

The systems we study in this work, a simple sphere and the NPoM, are axially symmetric if excitation (not always symmetric) is not included. Since in the calculation of quasinormal modes the excitation is not set yet, the calculations of the QNMs can be reduced to 2D simulations using this axial symmetry. This simplification strongly decreases the time required to simulate the QNMs. We discuss next how to modify the formalism described in subsection 5.1 to work with the QNMs calculated with the 2D simulations.

5.3.1 General principles

The quasinormal modes are given in this case in cylindrical coordinates ($E_r(r,z)$, $E_z(r,z)$, $E_\theta(r,z)$) and need to be expanded to three dimensions with the θ dependence given by $e^{im\theta}$. The electric field of the n^{th} QNM can be written as

$$\mathbf{E}_n^{3\text{D}}(r,z,\theta) = \mathbf{E}_n^{2\text{D}}(r,z)e^{im\theta} \ , \tag{39}$$

where the coefficient m is an integer number. Further, we express the incident electric field in cylindrical coordinates. For the plane wave considered in this section (z polarised and incoming in the x direction), the incident electric field in cylindrical coordinates is $\mathbf{E}_{\text{inc}} = E_0 e^{ikr\cos\theta}\hat{\mathbf{z}}$. The overlapping integral between the illumination and the QNMs (equation 39) can then be written as

$$I = \int_{V_{\text{res}}} \mathbf{E}_n \cdot \mathbf{E}_{\text{inc}} \mathrm{d}\mathbf{r} = E_0 \int_0^{2\pi} \mathrm{d}\theta \int\int e^{ikr\cos\theta} E_{n,z}^{2\text{D}}(r,z) e^{im\theta} \mathrm{d}r\mathrm{d}z \ , \tag{40}$$

where $E_{n,z}^{2\text{D}}$ is the z component of the electric field of the n^{th} 2D QNM. The integral in r and z variables is calculated following the script developed by the group of Philippe

Lalanne [20]. On the other hand, we evaluate the integral among the θ variable by using the trapezium rule,

$$I = \int_0^{2\pi} I(\theta)\mathrm{d}\theta = \frac{\Delta\theta}{2}\sum_{i=1}^{N}(I(\theta_{i-1}) + I(\theta_i)) \ . \tag{41}$$

Finally, to calculate the electromagnetic response using axially symmetric QNMs we must replace the overlapping integrals in equations 36 and 37a by the results from equation 41. For different illuminations than the one considered in this section we only need to change the expression for the incoming electric field in equation 40. To differentiate between the results of the previous subsection and the results obtained by exploiting axial symmetry, in the following we call them 3D QNM and 2D QNM calculations respectively.

5.3.2 Plasmonic nanosphere

We first calculate the quasinormal modes of the 30 nm radius sphere using 2D simulation with a similar mesh as in FEM simulations. In the axially symmetric calculation the modes are classified depending on the integer value m, which indicate the θ dependence (equation 39). In figure 10a we show 400 m=0 modes of the sphere distinguished by three colours. The red dots are the first three order modes of the plasmonic structure (the lowest-energy one is the dipolar mode and the others the quadrupolar and octopolar modes) and the blue dots the PML modes. The dipolar mode is three times degenerate, $m = 0, \pm 1$, but in the case of the z polarised plane wave only the $m = 0$ mode contributes to the results. In the case of the quadrupolar mode we have a degeneracy of five ($m = 0, \pm 1 \pm 2$), where only the modes $m = \pm 1$ contribute to the results when the plane wave is polarised in the z direction. In a similar way, the octopolar mode is seven times degenerate and only the $m = \pm 2$ modes have a non-zero contribution. Regarding to the PML modes, we have verified that only those with m=0 contribute significantly to the electromagnetic response. Thus, we consider only the m=0 PML modes in the following to optimise the calculations.

Comparing the quasinormal mode distribution calculated by axially symmetric simulations (figure 10a) to the 3D results from subsection 5.2 (figure 7a) we observe that they are very similar. However, in the 2D results we find some modes with almost zero imaginary part (green dots) that are not present in the 3D calculation, and that we call in the following continuous modes. Some green dots in figure 10a represent the higher order modes of the plasmonic structure, which are not distinguished from the continuous modes. The blue line in figure 10b shows the extinction cross section taking into account all the modes in figure 10a (including the continuous modes). We obtain a similar peak as in the FEM results at the position of the dipolar mode, but other narrow peaks also appear that are not present in 3D calculations. These narrow features are due to the continuous modes. Improving the mesh, more and more continuous modes are found, but their contribution becomes weaker. The orange line in figure 10b represents the extinction cross section but calculated with a better mesh than the initial one. We observe that we no longer obtain the large narrow peaks but some additional small resonances (compared to the 3D calculations) are still present. We do not understand yet the origin and nature of these modes, but our analysis seems to indicate that their contribution to the total electromagnetic response is only to produce the spurious narrow peaks. Thus, to get the

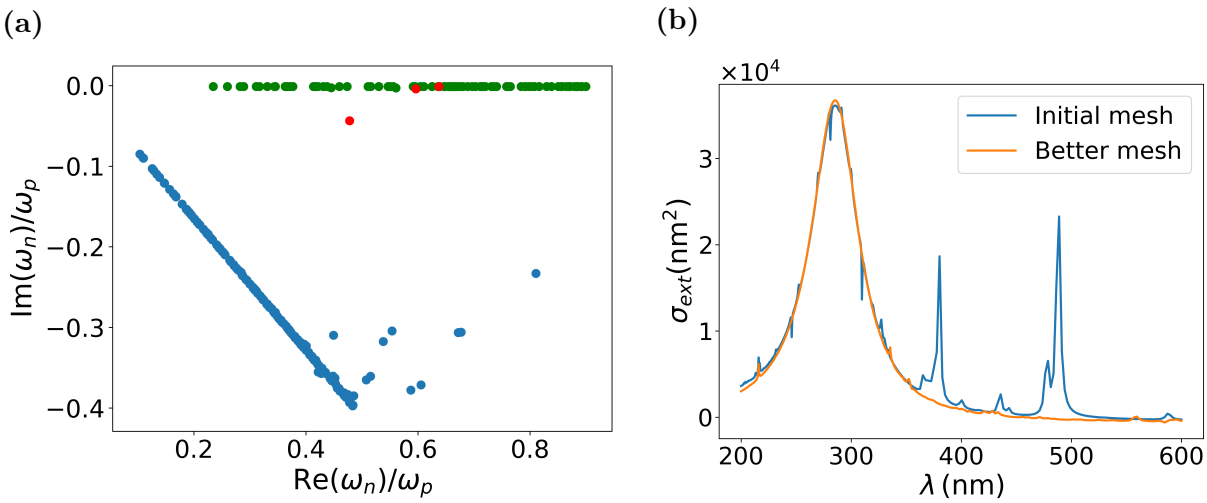

Figure 10: Results of the 2D QNM calculations for a 30 nm sphere (the permittivity is given by equation 38) surrounded by air and illuminated by a plane wave. (a) 400 modes of the sphere where the red dots are the first (lowest in energy), second and third order modes of the plasmonic structure, the blue dots are the PML modes and the green dots are the continuous modes (see main text). Only the modes with m=0 are shown since the modes for $m \neq 0$ have a similar distribution. (b) Extinction cross section including the contribution from all the calculated modes for $m = 0$ for different two meshes. The blue line is the result using a similar mesh as in the FEM calculation and the orange result is obtained with an improved mesh. The blue extinction cross section corresponds to the modal distribution displayed in (a).

final results for the sphere we do not calculate the continuous modes, which also saves significant computational time.

The main advantage of the axially symmetric calculations is that fewer discretisation cells are needed than for the 3D simulations. Thus, the calculations are much faster, allowing us to calculate more PML modes compared to subsection 5.2. In figure 11a 2000 PML modes with m=0 (blue dots) are shown along with the three main quasinormal modes of the plasmonic structure (red dots) for the converged mesh. In figure 11b we compare the extinction cross section for the sphere calculated with FEM (blue line) and calculated using the 2D QNM formalism (orange line) with the modes plotted in figure 11a. We see that the first resonance is well described by the 2D QNM result, although some discrepancies appear at high wavelengths. However, these differences between the FEM and QNM results are small (notice the logarithmic scale). Significantly, the differences are much smaller than for the corresponding 3D simulations (figure 9a), probably because of the larger number of PML modes used for 2D calculations. We think that the 2D QNM results can be further improved if more PML modes are calculated.

To better appreciate the contribution of the quadrupolar and octopolar modes to the extinction cross section, we show in figure 11c a zoom for small wavelengths of the extinction cross sections. We observe that with 2D QNM calculations (orange line) the second and third modes differ in a non-negligible manner from the FEM extinction cross section (blue line). Figure 11d shows similar effects in the z component of the field enhancement. In this case, there are no significant differences at large wavelengths between the FEM and 2D QNM results (contrary to the 3D QNM calculations in figure 9b), indicating that

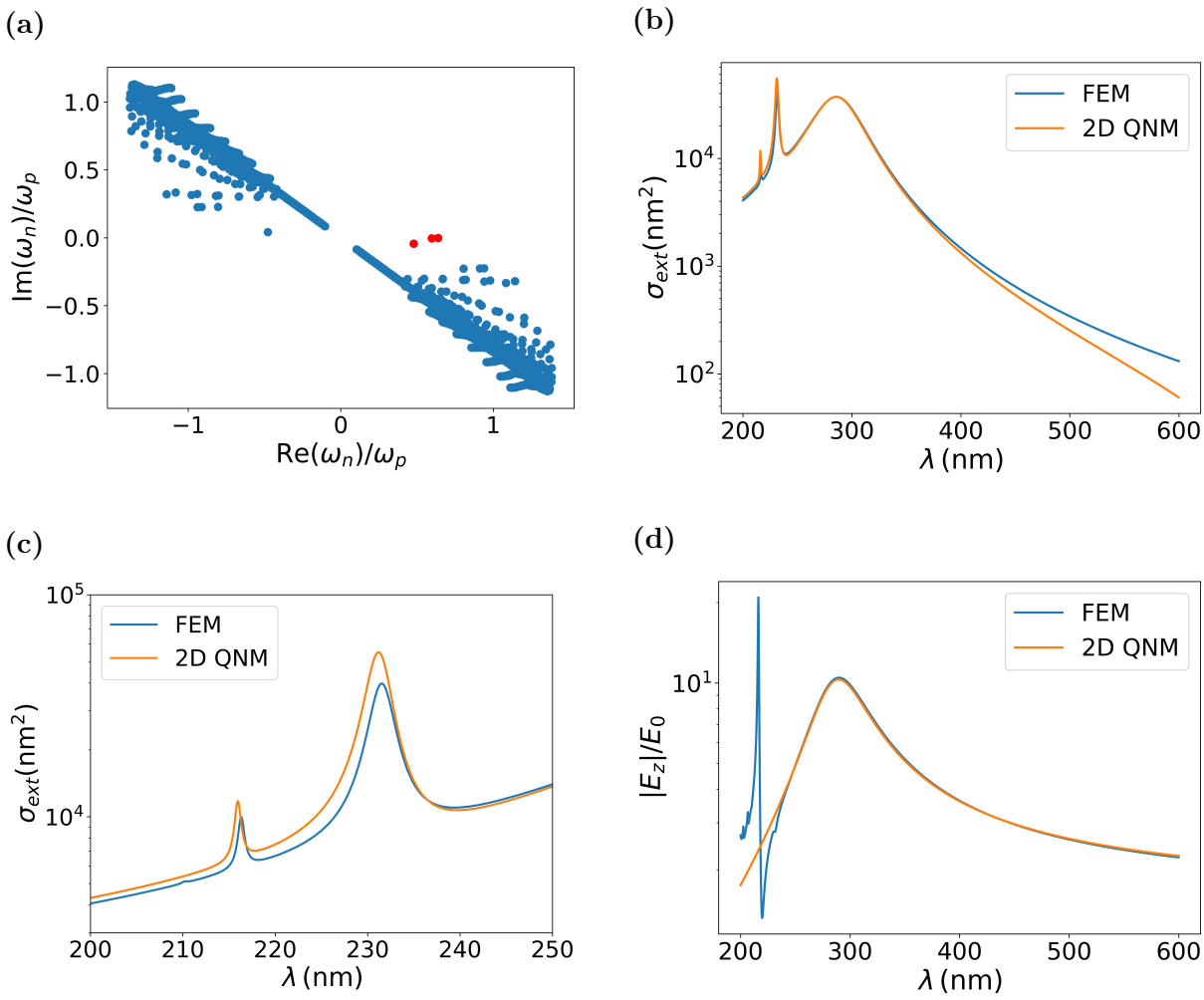

Figure 11: Results of the 2D QNM calculations for a nanosphere of 30 nm radius (the permittivity is given by equation 38) surrounded by air. In these calculations the continuous modes are not included. (a) 2000 m=0 PML modes (blue dots) and the three lowest-energy modes (dipolar, quadrupolar and octopolar modes) of the plasmonic structure (red dots). (b, c, d) Electromagnetic response calculated by FEM (blue line) and calculated by the 2D QNM formalism including the contribution of all the modes appearing in (a) (orange line) for a plane wave polarised in the z direction. (b) Extinction cross section and (c) zoom of the extinction cross section to the region where the quadrupolar and octopolar modes are found. (d) z component of the electric field enhancement ($|E_z|/E_0$) spectra at 2 nm from the surface of the sphere (z=32 nm).

the difference disappears when we take enough PML modes. However, there are no peaks for the wavelengths corresponding to the quadrupolar and octopolar modes. We believe that our approach for axially symmetric QNM calculations is not yet fully correct for modes with $m \neq 0$. Solving this issue requires further work, but we emphasise that 2D simulations can already be useful when we are mainly interested in the $m = 0$ modes. Further, it seems possible to combine 3D and 2D simulations, adding the PML modes calculated by 2D to the 3D results.

6 Quasinormal mode analysis of a nanoparticle on a mirror

We next use the QNM formalism to analyse the nanoparticle on a mirror (NPoM), which as explained in section 4 is a type of structure composed by a metallic nanosphere deposited in a metallic substrate with a nanometric gap between them (the exact geometry can be found in subsection 4.2 and in figure 4c). The NPoM is a very interesting plasmonic structure because it achieves a big field enhancement in the middle of the gap and it presents a complex response with many different modes [21]. We consider that the nanoparticle and substrate are made of gold, the most typical plasmonic material. As discussed in subsection 5.1, the formalism requires to use analytical permittivities to describe the materials. For gold, we specifically add a Lorentz term to the Drude model (appendix C). This permittivity is similar to the experimental one, but since they are not exactly the same, the FEM results that are used as reference in this section are calculated using the same Drude-Lorentz permittivity for gold (and are thus not identical to those in subsection 4.2). If required, more Lorentz terms can be added to the permittivity.

We follow the same process as in the study of the spherical nanoparticle. We first analyse the structure of the modes for the NPoM using the results obtained from the 3D QNM calculations. We show in figure 12a 200 quasinormal modes mostly associated with the plasmonic structure. The seven modes which contribute the most to the electromagnetic response are labelled with two numbers (lm). The first number (l) indicate if the mode is dipolar (l=1), quadrupolar (l=2) or a higher order mode and m represent its rotational symmetry in the vertical z axis (m can take any integer value between $-l$ and l). To identify the value of l and m for each mode we first analyse which modes of the plasmonic structure contribute most to the electromagnetic response. Afterwards, we select the modes with the largest contribution and analyse the field distribution near the nanoparticle in a similar way as in figure 6 (not shown). For example, the 10 (dipolar) and 20 (quadrupolar) modes correspond to the field distribution shown in figure 6. We do not calculate the PML modes, because to obtain converged QNM results for this complex structure we need very fine discretisation and the simulations take too long. We show below that it is still possible to obtain useful results with this simplification.

We plot in figures 12b and 12c the contribution of the different modes of the structure to the extinction cross section (figure 12b) and to the z component of the field enhancement in the middle of the gap (figure 12c). Only the modes with m=0 contribute to the field enhancement, whereas the modes with m=1 have a significant contribution (see legend) to the extinction cross section. We emphasise how using the QNM formalism for this system enables identifying the different modes and their individual contribution to the spectra quite straightforwardly. If only FEM simulations were used, it would be much more difficult to differentiate the modes because their resonances overlap strongly.

We compare in figure 13 the results obtained using FEM simulations (blue line) and using the QNM formalism (orange lines) including all the modes of figure 12a. The extinction cross section results (figure 13a) indicate that the QNM result is generally in good agreement with the FEM simulations, showing the same spectra features, although there are quantitative differences at low frequencies. Further, figure 13b shows that the QNM result for the z component of the field enhancement in the middle of the gap is in general

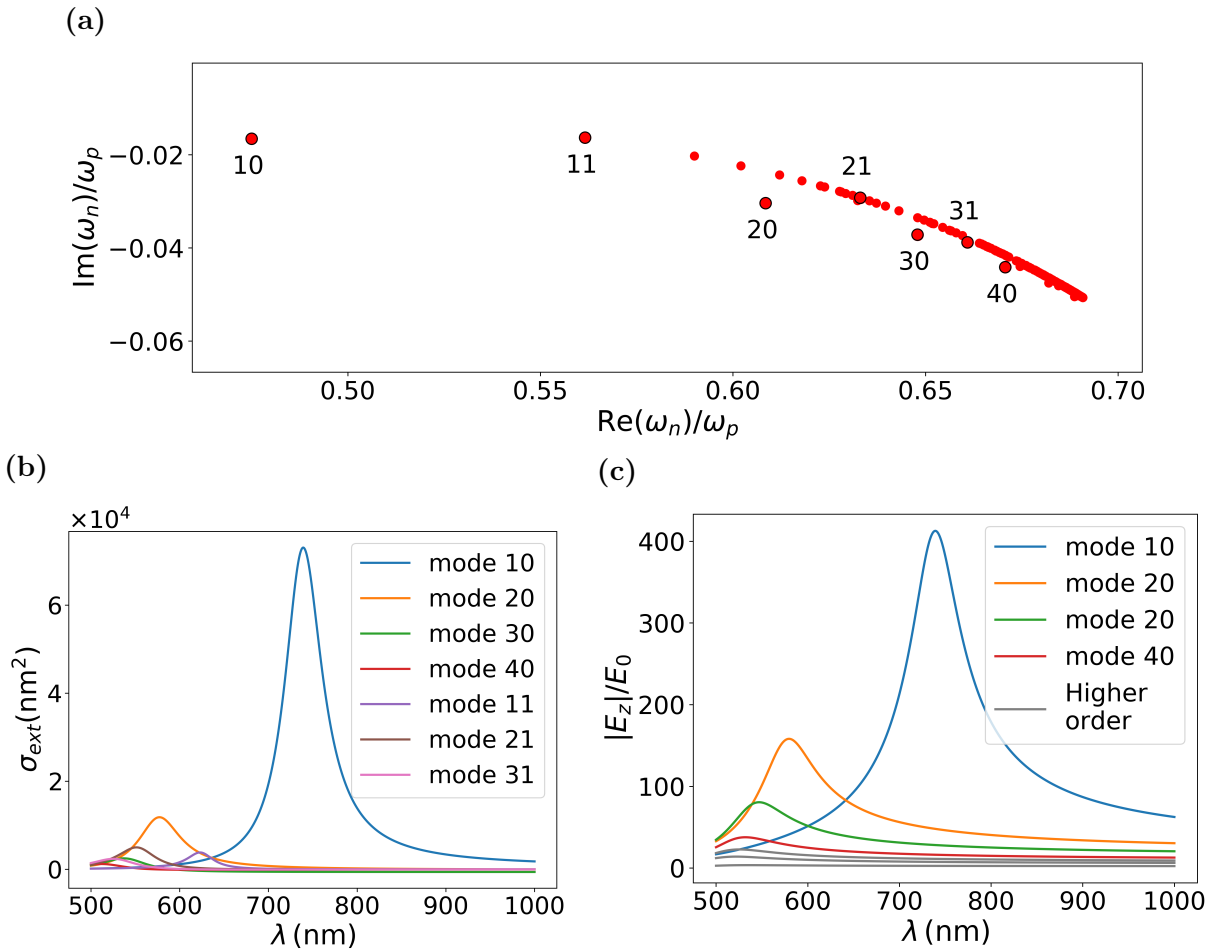

Figure 12: Analysis of the NPoM described in figure 4c using 3D QNM calculations. (a) Distribution of the 200 quasinormal modes of the plasmonic structure represented by red dots. We note that some of these dots may correspond to PML modes instead of modes of the plasmonic structure, as it can sometimes be challenging to distinguish between them. The seven modes of the structure that contribute the most to the electromagnetic response are surrounded by black outline and labelled with two numbers (lm). For the modes with m=1 we also have the modes with m=-1 at the same frequency. (b,c) Contribution of each mode (labelled in the caption) to the (b) extinction cross section and to the (c) spectra of the z component of the field enhancement (($|E_z|/E_0$)) in the middle of the gap.

very similar to the FEM calculations. Further, we also plot in figure 13 with dashed red lines the result of adding the contribution from the main modes identified in figure 12: modes 10, 11, 20, 21, 30, 31, 40 for the extinction and only the four modes with m=0 (10, 20, 30, 40) for the field enhancement. For the two cases we observe that the QNM results considering the contribution from all modes or only from the most important modes are very similar. This is advantageous since it indicates that it is possible to describe the NPoM results only with a few modes, which, for example, facilitates making analytical models.

We believe that the differences between the QNM and FEM results are because we are not taking the PML modes into account due to computational demand. Thus, we have also used the 2D QNM formalism to try to overcome this limitation. However, the effort has not been successful yet and it is discussed in the appendix D.

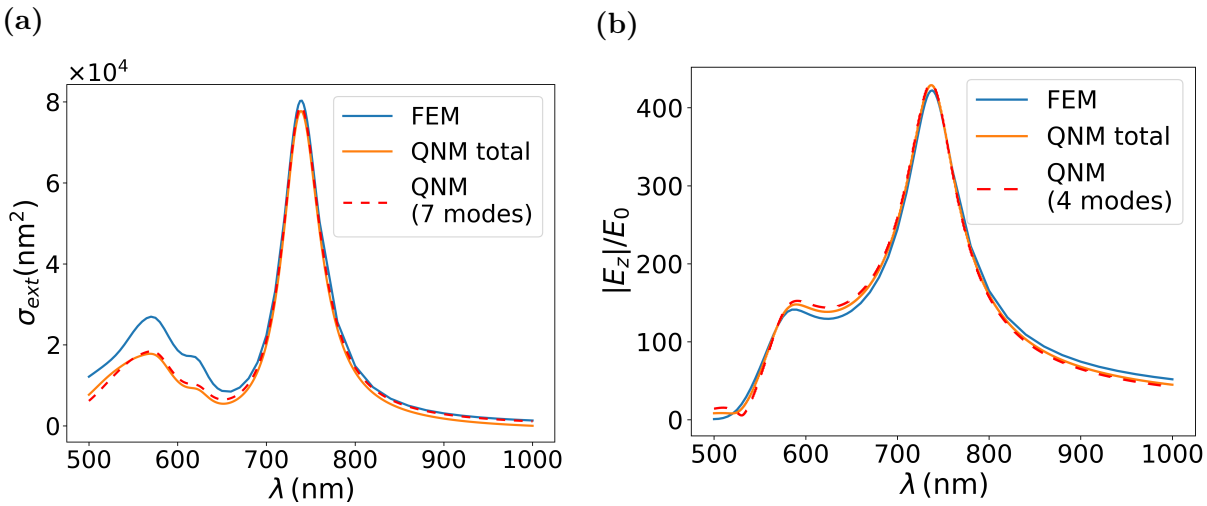

Figure 13: Comparison of the response of the NPoM described in figure 4c between the results obtained by FEM simulations (blue lines) and by QNM formalism including the contribution from all the modes in figure 12a (orange lines), or only the contribution from the main modes (red-dashed line). (a) Extinction cross section, where the red-dashed result is calculated using the modes labelled in figure 12a. (b) Spectra of the z component of the field enhancement ($|E_z/E_0|$) in the middle of the gap, taking only the four multipolar modes with m=0 and $l = 1, 2, 3, 4$ for the red-dashed result.

7 Summary and Conclusions

The main result of this thesis is the analysis of complex plasmonic structures using quasinormal modes QNMs. For this we have first discussed the basics of plasmonics using the quasi-static approximation for a small sphere, which allows obtaining a simple analytical solution. With this solution, we have shown that simple plasmonic structures increase and localise the electric fields near the metallic particle. Afterwards, we have discussed the finite element method (FEM), a numerical method that solves Maxwell's equations for any arbitrary complex structure. Comparing the FEM calculations to the analytical results obtained with the quasi-static approximation, we conclude that the approximation is valid for spheres with a radius smaller than ≈ 20 nm. For a bigger radius it is necessary to use simulations to obtain accurate results.

We have then considered a more complex structure including a nanometric gap, the nanoparticle on a mirror (NPoM). We have shown that the nanometric gap increases the field enhancement considerably compared to the single sphere, reaching enhancements of the order of 400. The bigger is the enhancement the stronger is the interaction between the plasmon and any material, such as molecules placed in the gap. This interaction facilitates for example the characterisation of the molecules, which shows that NPoMs are indeed promising plasmonic structures. Furthermore, we have identified two different dominant resonances in the electromagnetic response of the NPoM, the dipolar and quadrupolar resonances.

We can identify these two modes from the FEM simulations (in subsection 4.2) because the two resonances do not overlap spectrally too strongly. However, in many situations the identification of the modes is complicated. We have described and demonstrated the quasinormal mode formalism, which was recently introduced to simplify this task [7, 8]. We specifically use the approach of auxiliary fields and PMLs. We have introduced the basics of the formalism using as an example the response of a spherical nanoparticle. We show that we can represent quite well the electromagnetic response of the system by only taking few modes of the plasmonic structure. The differences between the FEM and QNM results are generally relatively small, illustrating the interest of the method, but some discrepancies remain. To reduce the differences, and considering that the geometry of the sphere is axially symmetric, we have used an alternative approach to work with QNMs in two dimensions. This formalism (which we call 2D simulations) enables the calculation of many more PML quasinormal modes. The improved agreement confirm the importance of the PML modes. However, the 2D simulations also represent some challenges: additional quasinormal modes (which we call continuous modes) appear that require special treatment and at this moment, it seems that we only describe well the response of m=0 modes. Despite these difficulties, the 2D simulations can lead to an important improvement when we mainly are interested in modes with m=0 symmetry.

Last we demonstrate the potential of the QNM formalism for analysing a real plasmonic structure often used in experiments, the nanoparticle on a mirror (NPoM). We are able to distinguish directly the contribution of each mode (even high order modes) to the electromagnetic response of this structure. Importantly, the analysis shows that we can describe the system quite well by only considering a few modes of the plasmonic structure. However, we face the same problem to reproduce the exact solution with the

QNM formalism as for the nanosphere system, because we are limited in the number of PML modes that we can calculate.

In conclusion, although we are not yet able to reproduce exactly the FEM results, our work confirms that the QNM formalism is a very interesting tool to analyse the electromagnetic response of complex plasmonic systems. Quasinormal modes are particularly useful when we are mainly interested in calculating the modes to understand the physics of the system, rather than obtaining directly the total spectra. A convenient approach could be to obtain a general understanding of the system with the 3D QNM calculations, and then use the 2D simulations to decrease the computational time and get more accurate results.

Different aspects of this work could be improved in the future. A first objective would be to analyse in more details the reasons for the discrepancies discussed above. Further, the permittivity of gold used in the QNM simulations could be improved by adding more Lorentz terms to describe better the NPoM. More generally, it would be interesting to use the QNM formalism to analyse other plasmonic structures in the context of practical applications. Further, molecules are usually modelled as dipoles, and thus it is also attractive to use QNMs to analyse the dipolar illumination. For example, a study of multiple molecules (multiple dipolar excitations) interacting with a plasmonic structure could be carried out very efficiently using the QNM formalism. Last, simplifying the total electromagnetic response in terms of a few resonances enables to make analytical models suited to study quantum effects.

Acknowledgements

This work is the result of the work I performed in the Theory of Nanophotonic Group[1] of the Centro de Física de Materiales (CSIC-UPV/EHU), led by Javier Aizpurua, and it has been supervised by Ruben Esteban, research scientist of CSIC. I want to thank Javier and Ruben for their help and commitment in the work and for giving me the opportunity to do this project with them. I would also want to highlight the help of Mario Zapata, a postdoctoral researcher of the group, Carlos Maciel, PhD student of the group and Yuan Zhang, researcher of Zhengzhou University (China). I also want to thank the Material Physic Center for hosting me to do the thesis. This work, which has been granted by a scholarship called *becas ikasiker*[2], gave me the opportunity to contribute in a paper about the importance of the full plasmonic response in Surface-Enhanced Raman Scattering studies [22].

[1] `https://cfm.ehu.es/nanophotonics/`

[2] `https://www.euskadi.eus/alumnado-universitario-becas-ikasiker-de-colaboracion/web01-a3lagun/es/`

Appendices

A Convergence study of the results

The FEM simulations require spatial discretisation and to limit the infinite space with perfectly matched layers. The better is the discretisation and the further away the PMLs the more similar is our simulated system to the real one. However, due to computational limitations, it is not possible to improve these factors arbitrarily. Therefore, before getting the final results it is very important to do a convergence study of the system, ensuring that our results do not change after improving the discretisation and the PMLs.

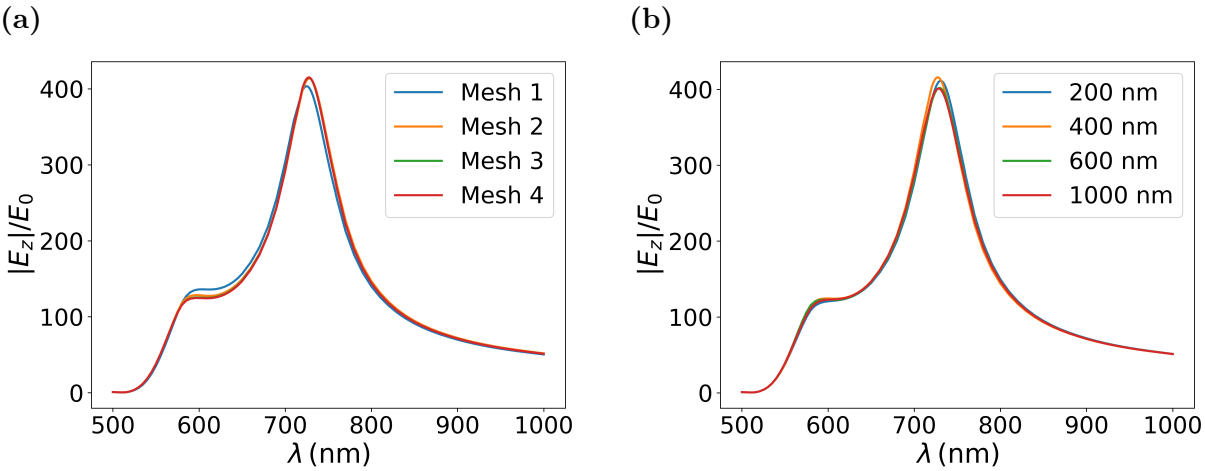

Figure 14: Two examples of the convergence study analysing the spectra of the z component of the field enhancement in the middle of the gap for the NPoM described in figure 4c. (a) Convergence study changing the nanoparticle mesh, where from the blue to the red line the mesh progressively improves. (b) z direction of the field enhancements ($|E_z|/E_0$) obtained by changing the radius of the PMLs. The blue line represents the smallest radius and the red one the biggest (see legend).

We present for illustration two convergence studies of the field enhancement in the middle of the gap obtained for the NPoM studied in subsection 4.2. We show in figure 14a results obtained for different discretisations of the NPoM. We observe that improving the mesh changes the result, but for the finer meshes (green and red lines) there is no appreciable difference, indicating that the system is well converged. Furthermore, we analyse in figure 14b the convergence as a function of the radius of the spherical PMLs. In this case, the simulations with the two biggest PML radius also give very similar results.

We note that the QNM results are not as well converged with respect to the PML size as those obtained with FEM. However, comparing QNM and FEM calculations indicates that the error is small and does not affect significantly the results of this work. Further, to ensure that the comparison of the QNM and FEM results is fair, the FEM calculations of sections 5 and 6 are done with the same size of the PML as in the QNM simulations.

B Electric field distribution for three layer systems

Due to computational reasons, when working with substrates in COMSOL it is favourable to define the background field (the illumination) as the results we would obtain without the nanoparticle. This background field is introduced in COMSOL using analytical equations, which we derive below using Fresnel coefficients.

When a plane wave illuminates an infinite interface between two different materials a fraction of the energy is reflected and the rest is transmitted to the second material (figure 15a). In this case, the reflected and transmitted waves are directly specified by Fresnel equations, which are derived from Maxwell's equations [10]. In our case, we consider an incident TM-polarised plane wave propagating in the xz plane, which is written as

$$\mathbf{E}_{\text{inc}} = E_0 e^{i(k_x x - k_{z1} z)} \hat{\boldsymbol{\mu}}_1 \ . \tag{42}$$

$\hat{\boldsymbol{\mu}}_1$ is the unitary vector of the polarisation of the incident electric field and k_x and k_{z1} are the x and z components of the wavenumber $|\mathbf{k_1}|$ of the incident plane wave.

We show in figure 15a the distribution of the waves for one interface system. The red arrows indicate the polarisation of the electric fields and the black ones the propagation of the waves. The reflected plane wave has the same propagation angle θ_{inc} as the incident plane wave, but with the opposite z direction. Therefore, the reflected electric field has the same polarisation as the incident one but with inverted x component (we indicate this polarisation with $\hat{\boldsymbol{\mu}}_{\text{r}}$). In the case of the transmitted field the angle of propagation θ_{t} and the electric polarisation (indicated by $\hat{\boldsymbol{\mu}}_{\text{t}}$) change. Specifically, the electromagnetic waves in each domain are

$$\begin{aligned} \mathbf{E}_1 = \mathbf{E}_{\text{inc}} + \mathbf{E}_r = E_0 e^{i(k_x x - k_{z1} z)} \hat{\boldsymbol{\mu}}_{\text{inc}} + r_{12} E_0 e^{i(k_x x + i k_{z1} z)} \hat{\boldsymbol{\mu}}_{\text{r}} \ , \\ \mathbf{E}_2 = \mathbf{E}_t = t_{12} E_0 \hat{E}_t e^{i(k_x x - k_{z2} z)} \hat{\boldsymbol{\mu}}_{\text{t}} \ , \end{aligned} \tag{43}$$

where r_{12} and t_{12} are Fresnel reflection and transmission coefficients, respectively, given by

$$r_{12} = \frac{\varepsilon_2 k_{z1} - \varepsilon_1 k_{z2}}{\varepsilon_2 k_{z1} + \varepsilon_1 k_{z2}} \ , \quad t_{12} = \frac{2 k_{z1} \sqrt{\varepsilon_1 \varepsilon_2}}{\varepsilon_2 k_{z1} + \varepsilon_1 k_{z2}} \ . \tag{44}$$

The wave numbers and its directions in each domain ($|\mathbf{k}_i|$, k_x, k_{zi}) are entirely specified by the permittivity of the materials (ε_i) once the incoming wave is defined,

$$|\mathbf{k}|_i = \frac{\omega}{c\varepsilon_i} \ , \quad k_x = |\mathbf{k}| \sin\theta_{\text{inc}} \ , \quad |\mathbf{k}_i| = \sqrt{k_x^2 + k_{zi}^2} \ . \tag{45}$$

Note that the difference between k_{z1} and k_{z2} correspond to the change from θ_{inc} to θ_{t}. Further, the unitary vectors of the electric fields are

$$\hat{\boldsymbol{\mu}}_{\text{inc}} = \frac{k_{z1}}{|\mathbf{k}_1|}\hat{\mathbf{x}} + \frac{k_x}{|\mathbf{k}_1|}\hat{\mathbf{z}} \ , \quad \hat{\boldsymbol{\mu}}_{\text{r}} = -\frac{k_{z1}}{|\mathbf{k}_1|}\hat{\mathbf{x}} + \frac{k_x}{|\mathbf{k}_1|}\hat{\mathbf{z}} \ , \quad \hat{\boldsymbol{\mu}}_{\text{t}} = \frac{k_{z2}}{|\mathbf{k}_2|}\hat{\mathbf{x}} + \frac{k_x}{|\mathbf{k}_2|}\hat{\mathbf{z}} \ . \tag{46}$$

In the case of the nanoparticle on a mirror we have a more complicate situation involving three different domains, air (domain 1), dielectric (domain 2) and metallic substrate (domain 3). We show in figure 15b the propagation direction of the plane waves in each domain (black arrows) and the polarisation of the electric fields (red arrows). In

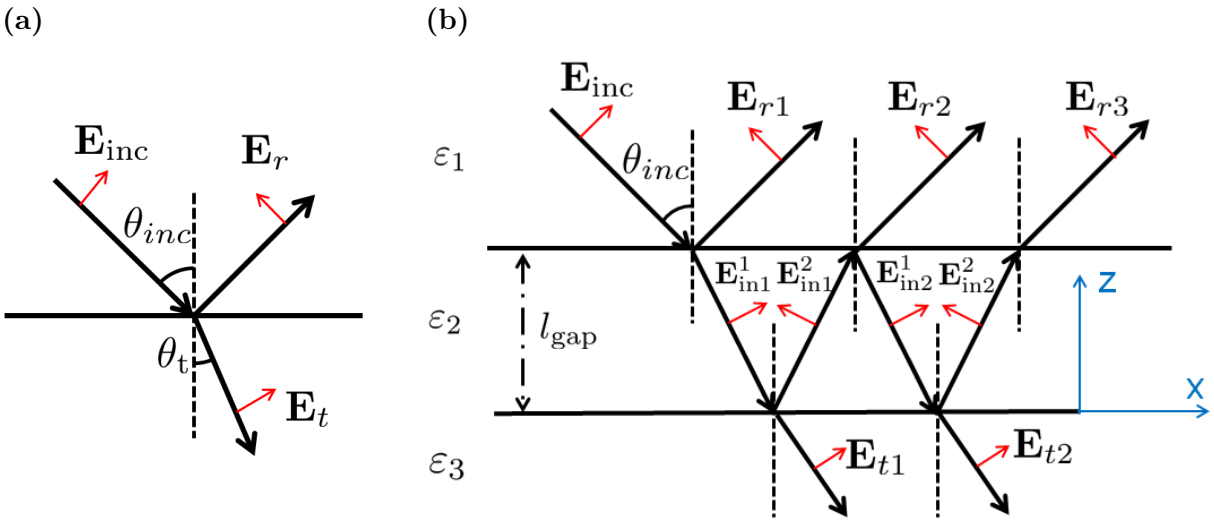

Figure 15: Sketch of the optical response of layer systems. The black arrows indicate the propagation direction of the plane waves and the red arrows the polarisation of the electric fields. (a) Reflection and transmission of an incident TM-polarised plane wave with electric field amplitude E_0 and incident angle θ_{inc} (with respect to the normal direction z). The corresponding propagation angle of transmitted light is θ_{t}. (b) Incident TM plane wave reflected and transmitted multiple time in a three domain system. To obtain the total electric field in each domain we sum over all reflected and transmitted waves. The coordinate axis used is indicated in (b).

this case, the plane in the dielectric layer is reflected infinite times, which produce interferences between the infinite plane waves. We can distinguish five different types of plane waves: The incident field ($\mathbf{E}_{\text{inc}}$), the reflected fields ($\mathbf{E}_{\text{r}}$), the transmitted fields ($\mathbf{E}_{\text{t}}$) and the fields propagating inside the dielectric layer in the negative and positive z directions ($\mathbf{E}^1_{\text{in}}$ and $\mathbf{E}^2_{\text{in}}$ respectively). We need to add these fields to obtain the total electric field in each domain,

$$\mathbf{E}_1 = \mathbf{E}_{\text{inc}} + \sum_{i=1}^{\infty} \mathbf{E}_{\text{r}i} \quad \mathbf{E}_2 = \sum_{i=0}^{\infty} \left(\mathbf{E}^1_{\text{in}i} + \mathbf{E}^2_{\text{in}i}\right) \quad \mathbf{E}_3 = \sum_{i=0}^{\infty} \mathbf{E}_{\text{t}i} \ . \tag{47}$$

Each field of figure 15b can be represented as

$$\mathbf{E}_{\text{inc}} = E_0 e^{-ik_{z1}(z-l_{gap})} \hat{\boldsymbol{\mu}}_1 \ ,$$

$$\begin{aligned}
\mathbf{E}^1_{\text{in1}} &= t_{12} E_0 e^{-ik_{z2}(z-l_{gap})} \hat{\boldsymbol{\mu}}^1_{\text{in}} \ , & \mathbf{E}_{r1} &= r_{12} E_0 e^{ik_{z1}(z-l_{gap})} \hat{\boldsymbol{\mu}}_{\text{r}} \ , \\
\mathbf{E}^2_{\text{in1}} &= t_{12} r_{23} E_0 e^{ik_{z2} l_{gap}} e^{ik_{z2} z} \hat{\boldsymbol{\mu}}^2_{\text{in}} \ , & \mathbf{E}_{t1} &= t_{12} t_{23} E_0 e^{ik_{z2} l_{gap}} e^{-ik_{z3} z} \hat{\boldsymbol{\mu}}_{\mathbf{t}} \ , \\
\mathbf{E}^1_{\text{in2}} &= t_{12} r_{23} r_{21} E_0 e^{2ik_{z2} l_{gap}} e^{-ik_{z2}(z-l_{gap})} \hat{\boldsymbol{\mu}}^1_{\text{in}} \ , & \mathbf{E}_{r2} &= t_{12} r_{23} t_{21} E_0 e^{2ik_{z2} l_{gap}} e^{ik_{z1}(z-l_{gap})} \hat{\boldsymbol{\mu}}_{\mathbf{r}} \ , \\
\mathbf{E}^2_{\text{in2}} &= t_{12} r_{23} r_{21} r_{23} E_0 e^{3ik_{z2} l_{gap}} e^{ik_{z2} z} \hat{\boldsymbol{\mu}}^2_{\text{in}} \ , & \mathbf{E}_{t2} &= t_{12} r_{23} r_{21} t_{23} E_0 e^{3ik_{z2} l_{gap}} e^{-ik_{z3} z} \hat{\boldsymbol{\mu}}_{\mathbf{t}} \ \ldots
\end{aligned} \tag{48}$$

Where r_{ij} and t_{ij} are the Fresnel coefficients from domain i to domain j given by equation 44, and the propagation and polarisation directions in each medium follow equation 45 and 46. In equation 48 the term $e^{ik_x x}$ is not written for simplicity.

Adding the infinite terms in equation 47 give the final analytical expression for the fields:

$$\mathbf{E}_1 = E_0 e^{ik_x x - ik_{z1}(z-l_{gap})}\hat{\boldsymbol{\mu}}_1 + E_0 e^{ik_x + ik_{z1}(z-l_{gap})}\left(r_{12} + t_{12}t_{21}\frac{r_{23}e^{2ik_{z2}l_{gap}}}{1 - r_{23}r_{21}e^{2ik_{z2}l_{gap}}}\right)\hat{\boldsymbol{\mu}}_{\mathrm{r}} \,,$$

$$\mathbf{E}_2 = E_0 t_{12} e^{ik_x x - ik_{z2}(z-l_{gap})}\frac{\hat{\boldsymbol{\mu}}^1_{\mathrm{in}}}{1 - r_{23}r_{21}e^{2ik_{z2}l_{gap}}} + E_0 t_{12} e^{ik_x x + ik_{z2}z}\frac{r_{23}e^{k_{z2}l_{gap}}}{1 - r_{23}r_{21}e^{2ik_{z2}l_{gap}}}\hat{\boldsymbol{\mu}}^2_{\mathrm{in}} \,,$$

$$\mathbf{E}_3 = E_0 t_{12}t_{23} e^{ik_x x - ik_{z3}z}\frac{e^{ik_{z2}l_{gap}}}{1 - r_{23}r_{21}e^{2ik_{z2}l_{gap}}}\hat{\boldsymbol{\mu}}_{\mathrm{t}} \,. \tag{49}$$

C Drude-Lorentz permittivity for gold

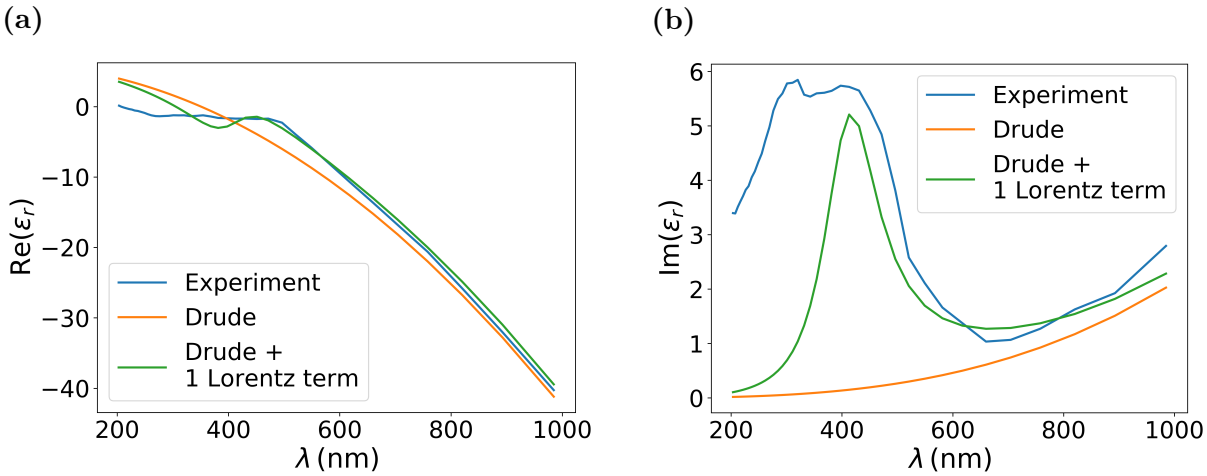

Figure 16: Comparison between the permittivity given by Johnson and Christy (blue lines) and the Drude-Lorentz model (orange and green lines) for gold. The orange lines represent the results obtained by using the simple Drude model and the green lines the permittivity obtained by adding 1 Lorentz term to the Drude model (equation 50). (a) Real part and (b) imaginary part of the permittivity.

The QNM formalism requires to use an analytical expression of the permittivity to describe the behaviour of the metals at complex frequencies. The permittivity of gold is not well described by the Drude model, and thus Lorentz terms need to be considered. The Lorentz terms describe interband transitions, which in the case of gold contribute more strongly to the permittivity for wavelengths λ around 500 nm. For the QNM calculations in this work the parameters given in [20] are used, according to which the permittivity of gold is described by adding only the first Lorentz term to the Drude permittivity,

$$\varepsilon_{r,\mathrm{Au}}(\omega) = \varepsilon_{\infty,\mathrm{Au}}\left(1 - \frac{\omega^2_{p,1,\mathrm{Au}}}{\omega^2 + i\gamma_{1,\mathrm{Au}}\omega} - \frac{\omega^2_{p,1,\mathrm{Au}}}{\omega^2 - \omega^2_{0,1,\mathrm{Au}} + i\gamma_{1,\mathrm{Au}}\omega}\right) \,. \tag{50}$$

The parameters we use that fit the analytical gold permittivity to the experimental values are

$$\varepsilon_{\infty,\mathrm{Au}} = 6 \,, \quad \omega_{p,1,\mathrm{Au}} = 5.37 \cdot 10^{15}\,\mathrm{rad/s} \,, \quad \gamma_{1,\mathrm{Au}} = 6.216 \cdot 10^{13}\,\mathrm{rad/s} \,, \tag{51}$$
$$\omega_{p,2,\mathrm{Au}} = 2.2636 \cdot 10^{15}\,\mathrm{rad/s} \,, \quad \gamma_{2,\mathrm{Au}} = 1.332 \cdot 10^{15}\,\mathrm{rad/s} \,, \quad \omega_{0,2,\mathrm{Au}} = 4.572 \cdot 10^{15}\,\mathrm{rad/s} \,.$$

In figure 16 the experimental permittivity of gold (blue lines) is compared to the results obtained from equation 50 (green lines) and given by a simple Drude model (orange lines).

The Drude model is obtained by only taking into account the first term (i=1) in equation 50. Figure 16a shows that the agreement between the experimental and modelled value of the real part improves significantly between $\lambda = 400 - 600$ nm regime if one Lorentz term is added to the Drude model. An even larger difference is found for the imaginary part of the permittivity. As it is shown in figure 16b, for the Drude model the imaginary part of the permittivity is very different from the experimental results, especially below $\lambda = 600$ nm wavelengths. Thus, for gold it is necessary to consider at least the first Lorentz term to approach the experimental results. If necessary, a better fitting can be obtained by adding more Lorentz terms to the permittivity.

D Implementation of axially symmetric simulations (2D calculations) for the NPoM

In section 6, we present 3D calculations of the NPoM. Here, we exploit the axial symmetry of the NPoM, which allows to reduce the problem to 2D calculations. With this aim, we follow the approach in subsection 5.3, but considering that the NPoM is illuminated by a plane wave that propagates at an angle with the normal of the substrate.

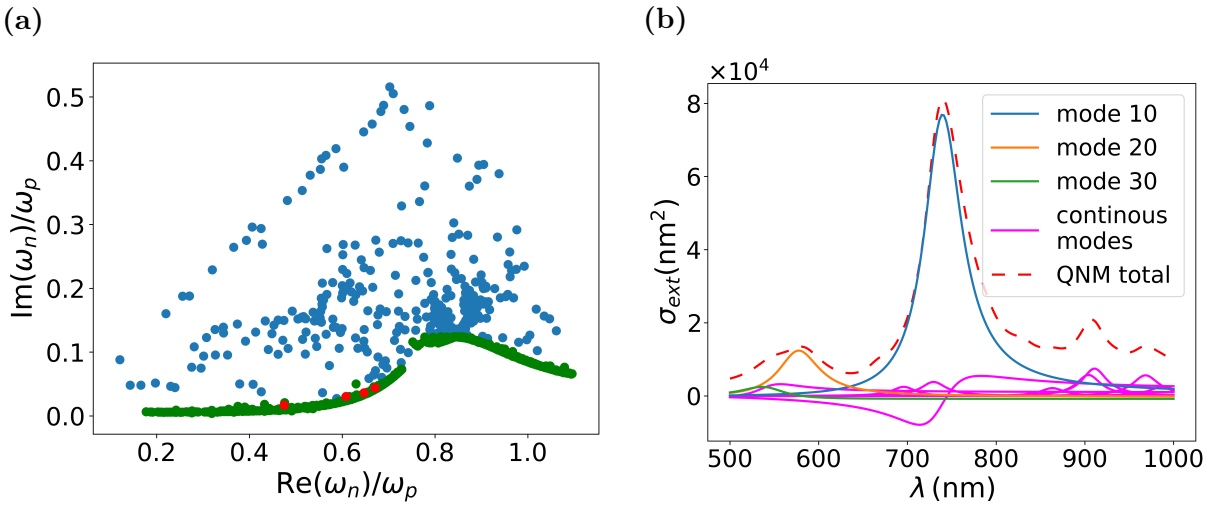

Figure 17: Results of the 2D QNM calculations for the NPoM system described in figure 4c. (a) Distribution of 2000 m=0 modes. The blue dots represent the PML modes and the four red dots the first, second, third and fourth order multipolar modes (10, 20, 30 and 40 modes respectively). The green dots correspond to either the continuous modes or to the modes of the structure that have little contribution to the final result. (b) Contribution to the extinction cross section of the modes in (a). The blue, orange and green lines represent the contribution of the 10, 20, 30 modes respectively, the magenta lines the contribution of few selected continuous modes and the dashed red line corresponds to the extinction summing all the modes. Similar results are obtained for $m = 1$ modes.

We show in figure 17a 2000 quasinormal modes corresponding to m=0 for the NPoM, calculated with the 2D QNM formalism using a mesh that is not fine enough to achieve convergence (the m=1 modes show a similar distribution). The blue dots are the PML modes and the red ones the first multipolar modes of the plasmonic structure. We can distinguish the first four multipolar modes of the structure (10, 20, 30, 40) by comparing

them to the results obtained with 3D simulations for the extinction cross section and field enhancement (figure 12). On the other hand, it is very difficult to distinguish between the continuous modes (modes that appear only in 2D simulations following a continuous pattern) and the higher order modes of the structure that contribute very little to the final result. Therefore, the green dots in figure 17a correspond to both the continuous modes and the higher order modes of the structure. We show in figure 17b the contribution of the most important modes of figure 17a to the extinction cross section. The contribution of the modes 10, 20, 30 is represented by the colours blue, orange, and green, respectively (the contribution of 40 to the extinction cross section is negligible). The magenta lines correspond to the resonances due to the continuous modes (only the modes that contribute most to the extinction are shown), which spectrally are relatively broad (contrary to the case of the sphere in figure 10b). We see that when we add the contribution of the continuous to the extinction cross section (red dashed line) the results worsen significantly comparing to the FEM simulations in figure 13a. Thus, we believe that it is convenient not to consider these continuous modes in the calculations of the spectra.

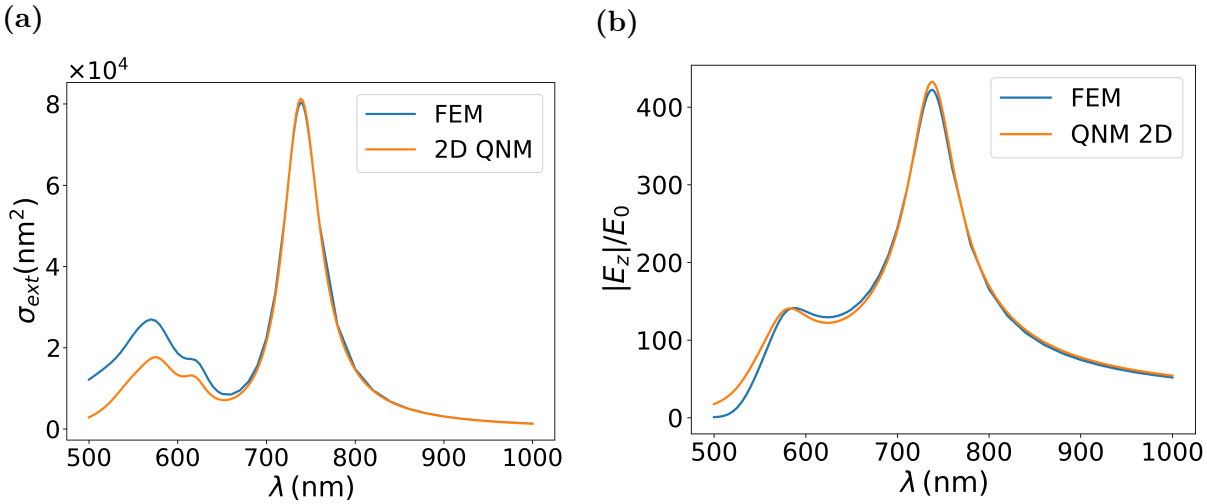

Figure 18: Comparison between the results obtained using the 2D QNM formalism (orange lines) and FEM (blue lines) for the NPoM described in figure 4c. Due to the difficulty to distinguish the modes of the structure from the continuous modes only the modes 10, 11, 20, 21 and 30 are considered. (a) Extinction cross section and (b) z component of the field enhancement ($|E_z|/E_0$) at the middle of the gap.

We compare in figure 18 the results obtained with the 2D QNM calculations (orange lines) and with FEM simulations (blue lines). In these calculations we refine the mesh (compared to the one used for figure 17) to achieve convergence. When we improve the mesh, more and more continuous modes appear (as in the sphere system) and the program did not find correctly the PML modes. In this case the contribution of the continuous modes to the electromagnetic response does not decrease improving the mesh. As discussed above, we neglect this contribution and focus on the modes of the structure. However, because the number of continuous modes increases when the mesh is improved we are no longer able to distinguish the 31 and 40 modes of the plasmonic structure. Thus, we only take the following modes for the 2D analysis: 10, 11, 20, 21, 30. For the extinction cross section (figure 18a) and the z component of the field enhancement in the middle of the gap (figure 18b) the resonant peak at $\lambda \approx 740$ nm due to the mode 10 are very similar in the FEM and QNM calculations. Indeed, the agreement in the extinction cross section is even better than for the 3D QNM calculations (figure 13a). At low wavelengths

the results obtained by the 2D QNM calculations are reasonably good, but we still observe some appreciable differences compared to the FEM results. We can identify several reasons behind these differences: (1) We are not calculating the contribution of the PML modes, (2) our 2D calculation does not seem to model correctly the $m \neq 0$ modes and (3) we do not identify all high order modes of the structure. Thus, further work is still necessary to better understand the 2D QNM simulations of the NPoM structures.

References

[1] M. Pelton, J. Aizpurua, and G. Bryant, "Metal-nanoparticle plasmonics," *Laser & Photonics Reviews*, vol. 2, no. 3, pp. 136–159, 2008.

[2] A. A. Maradudin, "Chapter 1 - introduction: Plasmonics and its building blocks," in *Modern Plasmonics* (N. Richardson and S. Holloway, eds.), vol. 4 of *Handbook of Surface Science*, pp. 1–36, North-Holland, 2014.

[3] D. J. de Aberasturi, A. B. Serrano-Montes, and L. M. Liz-Marzán, "Modern applications of plasmonic nanoparticles: From energy to health," *Advanced Optical Materials*, vol. 3, no. 5, pp. 602–617, 2015.

[4] K. Kneipp, "Surface-enhanced raman scattering," *Physics Today*, vol. 60, pp. 40–, 11 2007.

[5] G. Baffou and R. Quidant, "Thermo-plasmonics: using metallic nanostructures as nano-sources of heat," *Laser & Photonics Reviews*, vol. 7, no. 2, pp. 171–187, 2013.

[6] M. Pancaldi, N. Leo, and P. Vavassori, "Selective and fast plasmon-assisted photoheating of nanomagnets," *Nanoscale*, vol. 11, pp. 7656–7666, 2019.

[7] P. Lalanne, W. Yan, K. Vynck, C. Sauvan, and J.-P. Hugonin, "Light interaction with photonic and plasmonic resonances," *Laser & Photonics Reviews*, vol. 12, no. 5, p. 1700113, 2018.

[8] W. Yan, R. Faggiani, and P. Lalanne, "Rigorous modal analysis of plasmonic nanoresonators," *Phys. Rev. B*, vol. 97, p. 205422, May 2018.

[9] D. J. Griffiths, *Introduction to Electrodynamics*. Cambridge University Press, 4 ed., 2017.

[10] L. Novotny and B. Hecht, *Principles of Nano-Optics*. Cambridge University Press, 2 ed., 2012.

[11] N. Ashcroft and N. Mermin, *Solid State Physics*. Fort Worth: Saunders College Publishing, 1976.

[12] P. B. Johnson and R. W. Christy, "Optical constants of the noble metals," *Phys. Rev. B*, vol. 6, pp. 4370–4379, Dec 1972.

[13] J. D. Jackson, *Classical electrodynamics*. New York, NY: Wiley, 3rd ed., 1999.

[14] S. A. Maier, *Plasmonics: Fundamentals and Applications*. New York, NY: Springer US, 2007.

[15] "Analyze micro- and nano-optical devices with the wave optics module." `https://www.comsol.com/wave-optics-module`.

[16] M. G. Larson and F. Bengzon, *The Finite Element Method: Theory, Implementation, and Applications*. Berlin, Heidelberg: Springer Berlin Heidelberg, 2013.

[17] "The finite element method (FEM)." `https://www.comsol.com/multiphysics/finite-element-method?parent=physics-pdes-numerical-042-62`, March 2016.

[18] L. Saviot, "Javascript mie scattering calculator." https://saviot.cnrs.fr/mie/index.en.html.

[19] I. Romero, J. Aizpurua, G. W. Bryant, and F. J. G. de Abajo, "Plasmons in nearly touching metallic nanoparticles: singular response in the limit of touching dimers," *Opt. Express*, vol. 14, pp. 9988–9999, Oct 2006.

[20] P. Lalanne, "Light-in-complex-nanostructures/MAN: Versions 7.1 of QNMEig and QNMPole.." https://doi.org/10.5281/zenodo.3747453.

[21] N. Kongsuwan, A. Demetriadou, M. Horton, R. Chikkaraddy, J. J. Baumberg, and O. Hess, "Plasmonic nanocavity modes: From near-field to far-field radiation," *ACS Photonics*, vol. 7, no. 2, pp. 463–471, 2020.

[22] Y. Zhang, R. Esteban, R. A. Boto, M. Urbieta, X. Arrieta, C. Shan, S. Li, J. J. Baumberg, and J. Aizpurua, "Addressing molecular optomechanical effects in nanocavity-enhanced raman scattering beyond the single plasmonic mode," *Nanoscale*, vol. 13, pp. 1938–1954, 2021.